DESIGN AND ANALYSIS OF SILICONE GASKET SEALING FOR WATERPROOF PORTABLE SPEAKERS WITH THERMAL CREEP EFFECTS

By

BON WE UNG

A thesis submitted in partial fulfillment of
the requirements for the degree of

MASTER OF SCIENCE IN MECHANICAL ENGINEERING

WASHINGTON STATE UNIVERSITY
School of Engineering and Computer Science, Vancouver

MAY 2018

To the Faculty of Washington State University:

The members of the Committee appointed to examine the thesis of BON WE UNG find it satisfactory and recommend that it be accepted.

_____

Xiaolin Chen, Ph.D., Chair

_____

Dave Kim, Ph.D.

_____

Hua Tan, Ph.D.

ACKNOWLEDGMENT

First, I would like to thank my employer, Logitech, for the opportunity to work on portable speaker product design. Most of the design, analysis, and testing was conducted on Logitech grounds, using their Ansys simulation resources and lab test equipment.

I would also like to thank my advisor Dr. Xiaolin Chen, who guided me throughout the thesis writing process, and Dave Kim and Hua Tan for their service on my committee.

DESIGN AND ANALYSIS OF SILICONE GASKET SEALING FOR WATERPROOF PORTABLE SPEAKERS WITH THERMAL CREEP EFFECTS

Abstract

by Bon We Ung, M.S.
Washington State University
May 2018

Chair: Xiaolin Chen

As consumer electronics are becoming more portable, they are exposed to more potentially damaging conditions such as temperature extremes and water exposure. The purpose of this research is to document the design and analysis process involved in waterproofing a portable speaker product and the challenges encountered, which has not yet been done. Computer simulation is used to optimize the gasket sealing performance of the speaker during its product development, while considering its particular design constraints. The constraint that is most challenging to meet is maintaining sealing after exposure to 70°*C* heat. The sealing performance after thermal creep effects is analyzed both through simulation and experimental testing. Ultimately, the optimized gasket design proved capable of surviving thermal exposure despite variations in the manufacturing process. Sealing surface imperfections was also analyzed and it was found that hairs as small as 50 microns could greatly affect sealing performance, necessitating air blower cleaning and finished product air leak checks. The failure analysis also highlights that air leak rates and water tightness are not 100% correlated. Engineers seeking to waterproof their products may benefit from this research.

TABLE OF CONTENTS

Page

LIST OF TABLES

Page

LIST OF FIGURES

Page

CHAPTER ONE: INTRODUCTION

As consumer electronics are becoming more portable, they are exposed to more potentially damaging events such as temperature extremes and water exposure. These potentially damaging events decrease the average life of the product and therefore decrease the value to the customer. For the product category of premium wireless Bluetooth speakers, it makes economic sense to invest in product waterproofing features. Waterproof portable electronics have proved invaluable for consumers who are expected to stay in wet environment for a long period of time. The future growth of the portable electronics industry is influenced by the products' performance and lifespans, and consequently reliable waterproofing technology plays a critical role in advancing mobile technology.

Consumer electronics must be protected from water as water can short circuit printed circuit board (PCB) components and cause permanent damage, possibly creating a non-operating device and needless waste. Therefore, PCBs must be designed such that they exist in volumes that are separated from the volumes which water can exist. This separation of volumes may be achieved in a number of ways with the simplest method being a solid impermeable wall. However, since electronic housings are typically formed by several parts, at the interface between these parts, there exist small gaps that water may flow through. Fig. 1 diagrams the basic sealing problem and depicts two fluids. These gaps, as shown in Fig. 1, may be closed off through the application of rubber gaskets inserted into the interface. Rubber gaskets are not only one of the most tested sealing technique, but also one of the most varied types of gaskets. Besides the cost benefit, there are many other advantages of using rubber over metallic or other non-metallic gaskets such as their outstanding sealing properties and excellent temperature stability in extreme environments. When rubber gaskets are placed into an interference fit design,

the resulting contact pressure deforms the rubber to fill any gaps. Interference gasket seals are favored because the seal is easier to install and disassembly is non-destructive compared to adhesive seals.

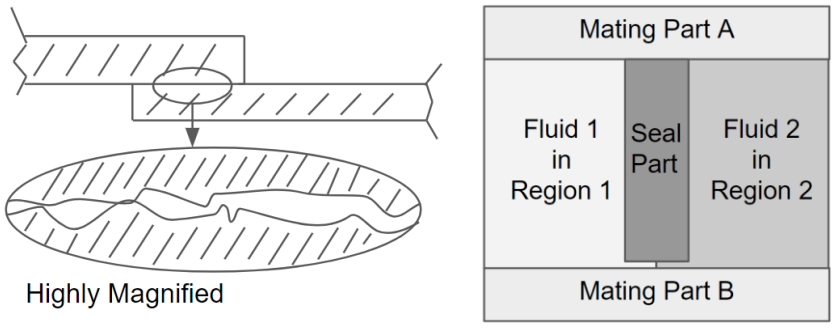

Fig. 1. The basic sealing problem [1]

Waterproof may be advertised on product packaging and usually indicates a level of water protection that is higher than water resistant. To design a waterproof system, first the term "waterproof" must be clarified. There are several grades of water protection, standardized by the IP scale (ingress protection rating) as shown in Table 1. The water resistant protection level corresponds to water IP ratings 1-6, which describe spraying of water onto the product from various directions, distances, pressures, and durations. The waterproof protection level corresponds to water IP rating 7 or higher, which describes water immersion of the product at one meter depth for thirty minutes. There is another range of values for describing solid ingress protection, which is not considered here. As such, the IP design target is called "IPX7" with the "X" signifying that the dust protection (solid particle ingress) is undefined.

Table 1. International Electrotechnical Commission (IEC) Standard-IP Ratings Guide [2]

Water Protection Rating:	Description:
IPX1	Protected against vertically falling drops of water. Limited ingress is permitted.
IPX2	Protected against vertically falling drops of water with enclosure tilted up to 15 degrees from the vertical. Limited ingress permitted.
IPX3	Protected against sprays of water up to 60 degrees from the vertical. Limited ingress permitted for three minutes.
IPX4	Protected against water splashed from all directions. Limited ingress permitted.
IPX5	Protected against jets of water. Limited ingress permitted.
IPX6	Water from heavy seas or water projected in powerful gets shall not enter the enclosure in harmful quantities.
IPX7	Protection against the effects of immersion in water at 1 m depth for 30 minutes.
IPX8	Protection against the effects of immersion in water under pressure for long periods.

When considering speaker products and the IPX7 rating, the two fluids of interest are typically fresh water and air. The air volume is internal and necessary for sound creation. The water volume is external and at one meter depth has a pressure of 0.01 M*Pa*. When the product is immersed in water, the pressure will act to compress the product, as well as force water into the product if any entry paths exist. The parts of the product must be dimensionally controlled such that gaps are not created as a result of assembly tolerances. It is worth noting that in Fig. 1 a small gap is shown between the seal part and mating part B. This gap would allow fluid to flow from one region to another, which is acceptable for some applications where a small leak limit is allowed, but not acceptable for an IPX7 rating, where no water ingress is allowed. Hence, the seal part must always be in a compressed state.

As with all products, the cost of components is an important factor. Plastic-injection-molding is typically the most economical method of manufacturing for high volume production (100,000+ parts). The most economical and most commonly available plastic is Acrylonitrile-Butadiene-Styrene (ABS), which is a thermoplastic polymer material. For many structural

applications, this material is sufficiently stiff, strong, light, and affordable, making it an ideal candidate for use in wireless speakers. Therefore, the two mating surfaces shown in Fig. 1 will be considered as ABS material. However, while ABS is easy to process as a thermoplastic, this same material characteristic makes it susceptible to thermal creep. Although most consumers will typically use their speakers indoors, there are times when the speaker product may be exposed to unusually high or low temperatures. During product transport from the factory to the distribution center, the product may be exposed to cold and hot temperatures as it travels across the ocean on freighters. Or if the consumer leaves the product in their vehicle, the greenhouse effect may raise the temperature of the product significantly. Therefore, speakers must be designed to be resilient under temperatures as high as $70°C$. The challenge of using thermoplastics, which are easily melted to be molded into the desired shape, is that these materials are also easily softened by temperatures of $70°C$. In the softened state, if a force is applied, such as the force created by an interference seal, the ABS material tends to undergo permanent deformation. This deformation is termed creep or cold flow. When components creep, gaps have the potential to form, allowing for water ingress, and therein lays the design challenge.

Despite the important role of waterproofing for consumer electronics, there were very few publications that described how to design seals specifically for waterproofing portable consumer electronics. Lee et al. [3] simulated the gasket sealing performance of an engine cylinder head under several thermal loading conditions, considering the effects of thermal expansion but not material creep. Bao et al. [4] provided simulation results of a shape memory alloy (SMA) gasket seal, considering how temperature fluctuations affect the SMA seal. The materials used in Bao's seal design were metal and glass. Yun et al. [5] studied the sealing contact characteristics of subsea collet connectors, composed of metal and without consideration of creep effects.

Bharadwaj et al. [6] simulated the creep of polytetrafluorethylene seals compressed between bolted metal flanges. There have also been numerous publications on sealing in general [7-21], considering both static and dynamic seals acting to seal joints of various geometries. However, these seal designs often permitted some level of leakage and addressed temperature extremes by using high temperature materials such as metal. In this work, the design materials are restricted to silicone rubber and Acrylonitrile-Butadiene-Styrene (ABS) plastic for cost reasons. The focus will be on an interference rubber gasket seal design with consideration for thermal creep effects, where it is the flanges and not the seal that undergo creeping displacement behavior.

This research details the design constraints involved with waterproofing a wireless speaker using a gasket interference design, as well as the solutions obtained with the aid of FEA simulations. The purpose of the research is document the solution process so that other engineers can understand the key problems encountered and how to overcome them. The research is organized as follows. Chapter 1 introduces the key design problem to overcome as well as the motivating factors for solving the problem and its importance for the portable electronics industry. Chapter 2 explains the background information including the general sealing problem, challenges, and working principles. Chapter 3 describes the design constraints, the material properties and method of approach as it applies to a case study. Chapter 4 describes the simulation set up and results. Chapter 5 describes the testing methods that are used not only to validate the simulation results but also to test IPX7 performance. Chapter 6 analyzes the influence of surface defects on sealing performance and mitigation steps. Chapter 7 provides concluding remarks.

CHAPTER TWO: SEALING BACKGROUND

Water protection for mobile speakers may come in many forms, including adhesives, welding, and foams. This research will focus on the rubber or elastomeric gasket seal option. The elastomeric seal is relatively compliant. The required hardness and elasticity will depend on the particular sealing system. These rubber seals may be formed through compression molding or over-molding onto the mating parts that are to be sealed. Many materials may be selected from for use as a gasket seal. The ideal gasket seal shape and material must meet many requirements. The seal design must be easy to manufacture, affordable, easy to assemble, resistant to twisting, extrusion pressures, corrosion, and compression set, but also compliant enough to conform to rough surfaces or surface irregularities such as dust and fiber particles.

Many of the goals can be met by working with a gasket manufacturer to select the appropriate material and shape. Following standard guidelines for simple geometries such as the O-ring seal, an engineer can design basic sealing systems. An example of a basic sealing system would be a ‘face’ seal where an O-ring gasket is clamped between two faces and those faces are screwed together. More complex sealing systems require more analysis and development work. To optimize the sealing system behavior would typically require trial and error methods with physical parts that can be very costly and very time consuming. Simulation of mechanical behavior has become more viable in recent years. Simulation offers the engineer the ability to analyze the sealing system as well as make geometry iterations to arrive at an optimized solution. Optimized solutions meet goals such as minimal use of materials, minimal use of space, low cost, ease of manufacture and assembly, and robust performance under operating conditions over the lifetime of the product.

Seals may fail over time and/or through exposure to high or low temperatures. Pinpointing the time and location of sealing failure can be quite difficult to do with physical samples. Seals are often internal which means that visual inspections require product disassembly, which breaks the sealing system. Therefore, visual inspection of sealing failure and testing of the sealing system performance cannot happen at the same time. This makes it very difficult to see where a sealing failure is coming from. Simulation tools can facilitate the failure analysis since the software allows for hiding parts and creating cross section views. Sealing failure locations may be observed as the places where sealing contact pressure is too low. Failures may even be identified more obviously as air gaps between mating parts. More importantly, simulation can aid the design process by preventing faulty designs early, reducing the number of failure analysis cycles.

Seals may fail over time because plastic parts tend to creep with time and temperature. The greater the compression on the gasket needed to create the sealing pressure, the greater the potential for plastic creep strain to increase. After some time, the creep strain may be enough to compromise the seal. The goal of gasket seal design for consumer electronics is to manage the plastic creep stain enough such that the seal will not fail over the life of the product, which is 3 to 5 years.

To further understand the IPX7 requirement, the water pressure is calculated. When submerged under water at a depth of 1m, the hydrostatic pressure, $p = \rho gh$, where ρ is the density of the fluid (water's density = $1 g/cc$), g is the gravitational constant ($9.81 m/s^2$), and h is the depth of the water ($1m$). Then hydrostatic pressure, p is approximately $0.01 MPa$. To prevent this fluid pressure from breaching a seal, the seal's contact pressures must be greater than the hydrostatic pressure. Oftentimes a safety factor between 1 and 2 is sufficient. If the pressure of the fluid

being contained does not exceed the contact stress or pressure of the O-ring, leaking cannot occur [10]. Fluid pressure is often used to supplement the contact pressure. In this way, when fluid pressure is higher, the contact pressure is also higher and maintains the seal [22]. In Fig. 2, notice how the fluid pressure acting on the left side of the seal body, would tend to increase the sealing pressure on the top and bottom of the seal body through the Poisson's effect in the case of elastic seals. In fact, the resulting sealing pressure is the sum of the initial sealing pressure and the fluid pressure.

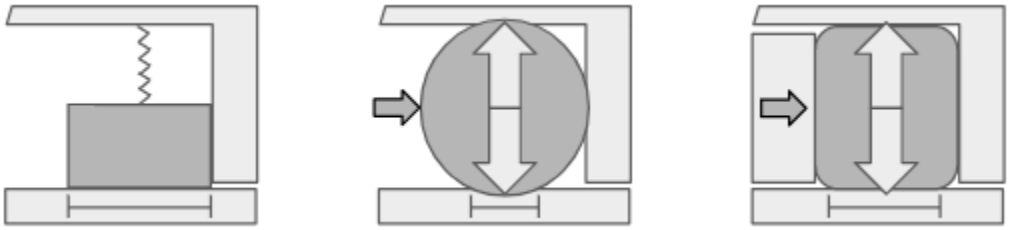

a) Separate spring load b) elastic seal with interference c) plastic seal with axial load

Fig. 2. Seal bodies preloaded to create sealing pressure [22]

Another concept to be mindful of is the contact width between gasket and sealing surface. In a 3D representation of the seal system, the contact width is actually a contact surface area, but in the 2D cross section representation, the contact width is a linear dimension as marked below each seal body in Fig. 2. Higher compressive forces will increase the contact width. Smoother surfaces also increase the contact width, while rougher surfaces decrease the contact width [11]. When the gasket contacts a rough surface, only a fraction of the gasket surface is in contact with the rough surface. Therefore, the effective contact width is the sum of the individual contact widths.

The smaller the total contact width, the greater will be the potential for leakage, since small pieces of debris such as dust and fibers may happen to occupy the regions intended to be contact

surfaces, creating air gaps and causing sealing failure. Larger contact widths are more tolerant of debris since the seal would surround small debris. However, excessive contact widths will increase compressive forces that could lead to gasket damage or creep of the mating surfaces, since compressive force is the product of sealing pressure and sealing area.

CHAPTER THREE: SEAL DESIGN CRITERIA AND CONSIDERATIONS

Based on the general guidelines for sealing in literature, a sealing checklist may be formulated. The success of static seals may be achieved by meeting the following criteria:

Criteria 1: **Gasket material is compliant enough to seal over surface irregularities such as roughness, dust, fibers, etc.** This requires searching materials and properties, verifying compliance, and designing a sufficiently wide contact surface.

Criteria 2: **Gasket material is stable under expected range of operating temperatures.** This requires searching material and properties, verifying mechanical properties under $70°C$ conditions.

Criteria 3: **Gasket material experiences low compression set at $70°C$.** Again, this requires searching material and properties and selecting a material with sufficiently low compression set.

Criteria 4: **Gasket geometry is resilient to positional tolerances.** For example, if the gap between two surfaces to be sealed is oversized by $0.2mm$, the gasket sealing pressure should not drop low enough to cause sealing failure. This is important for maintaining a reliable seal, that is, a seal that always functions in spite of manufacturing variability. Additionally, if the surfaces to be sealed have gap decreased by $0.2mm$, the gasket sealing pressure should not rise high enough to damage the gasket or plastic parts. This will be discussed further in criteria 6. Achieving a tolerant gasket geometry requires simulating the compression behavior with compression gap +/- $0.2mm$. The material models must be accurate.

Criteria 5: **Gasket geometry resists twisting and displacement.** This is important to prevent improper assembly of the gasket. Gaskets that are overly compliant may fall out of position as the two sealing surfaces are brought together by hand assembly. This also includes

checking to see what happens if the gasket were over-compressed before being installed at the correct compression gap. The assembly process must be well understood by both engineer and operator. Vibration and impact loads must also be considered to prevent gasket displacement. Adhesives may be used to prevent gasket movement.

Criteria 6: **Sealing surfaces must be able to tolerate the sealing forces**, meaning the resulting creep strain at 70°*C* is within an acceptable limit. Ideally, the sealing surfaces are stiff enough to maintain a sufficiently high compression pressure even after creep strain. The stiffness of the sealing surface structure may be increased following the laws of structural mechanics. This includes using materials with high Young's modulus, stability under operating temperatures, and low creep rate. For structural stability, the primary parameters are beam thickness and beam lengths. The simulation must consider creep effects at 70°*C* for ~100 hours or whenever the creep effects have stabilized. Structural stability may also be augmented by adhesive joining but adhesives complicate disassembly processes so it is not the preferred solution.

Seal materials must be chosen carefully. Polymeric seals include both elastomeric and plastic materials. Elastomers are more often used for sealing purposes than plastics. Elastomers have several properties that make them suitable for sealing bodies. Their low elastic modulus and large elongation-to-break allow them to withstand large interference fits without damage. Their high Poisson ratio makes them essentially incompressible. Fluid pressure can be transmitted in all directions. Low shear modulus allows them to change shape without loss of volume. This explains why elastomeric O-rings basically become rectangular when compressed into a rectangular groove.

In general, other material characteristics must be checked. Glass transition temperature effects must be considered since elastomers begin to lose their elasticity at such temperatures. Fluid uptake is also something to consider since excessive swelling can lead to gasket displacement. Chemical attacks and temperature aging are a concern as well. Compression set of the elastomeric seal would lower the contact pressures and impair the sealing performance. The compression set is measured in the linear interference dimension, between a seal and its mating faces. Compression set can range from 0 to 100% where 100% is complete loss of interference pressure. Different elastomers will have differing combinations of properties so the best polymer will vary depending on the requirements of the product.

In this case study, silicone rubber is selected for the seal body. Silicone rubber is made from raw silicone rubber gum and high-purity silica. Silicone rubbers have fine electrical properties, good chemical stability and flame retardancy, and excellent resistance to heat and cold [23]. Siloxane bonds are highly stable (-Si-O-Si-). This is responsible for the higher heat resistance and chemical stability. Low intermolecular force and high coil formation capacity allow the polymer chains to be highly elastic, highly compressible, and resistant to cold temperatures. Silicone rubber is also hydrophobic and therefore water repellant. Silicone spray-on coatings have been used to waterproof parts. These coatings have low surface tension which allows them to spread and soak easily into porous surfaces. Due to the molecular structure, water molecules cannot penetrate through a silicone barrier but water vapor may pass back and forth. Silicone rubbers do not become brittle above -60°*C*, which makes them highly durable. Silicone has great weatherability with its physical properties unchanged after exposure to wind, rain and UV rays for extended time periods [23]. Silicone rubber is also very resistant to steam and other chemicals. Low compression-set values are important characteristics for gasket seal stability. As

can be seen in Fig. 3, compression set values are under 5% at the 70°*C* , as well as at 100°*C*. Low creep values are also critical for sealing (Fig. 4).

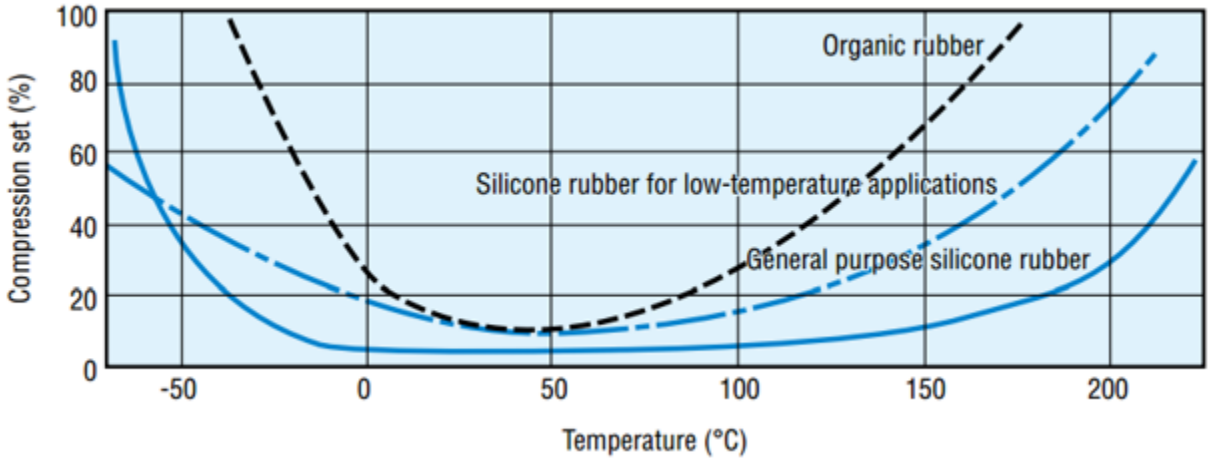

Fig. 3. Silicone compression set values at various temperatures

(test conditions: 22 hours at each temperature) [23]

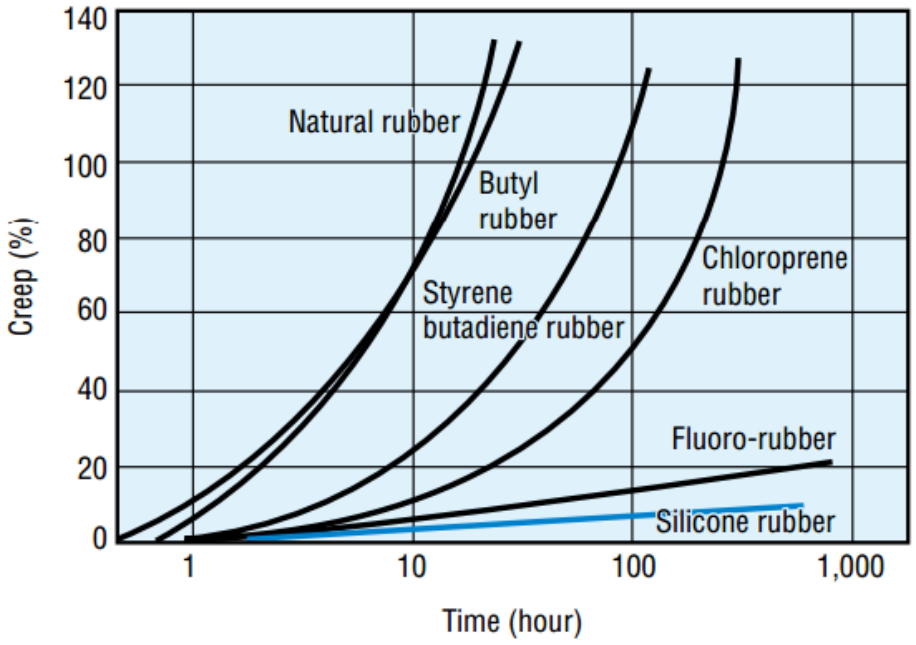

Fig. 4. Silicone creep values [23]

To consider gasket geometry further, gaskets placed in a groove must not be overfilled to prevent extrusion damage or jamming. The maximum volume filling should not exceed 95% of the groove volume [24]. Refer to Fig. 5 for an illustration of axial and radial interference seal designs. Groove width is generally sized to be 15% larger than the O-ring cross-sectional diameter, to allow the cross section to flatten into an oval shape. Thermal expansion of the gasket cross section must also be considered. In the case of silicone, a 50 centigrade increase from 20°*C* to 70°*C* results in a 1% size increase per linear dimension [25], which is small enough to be neglected in simulation.

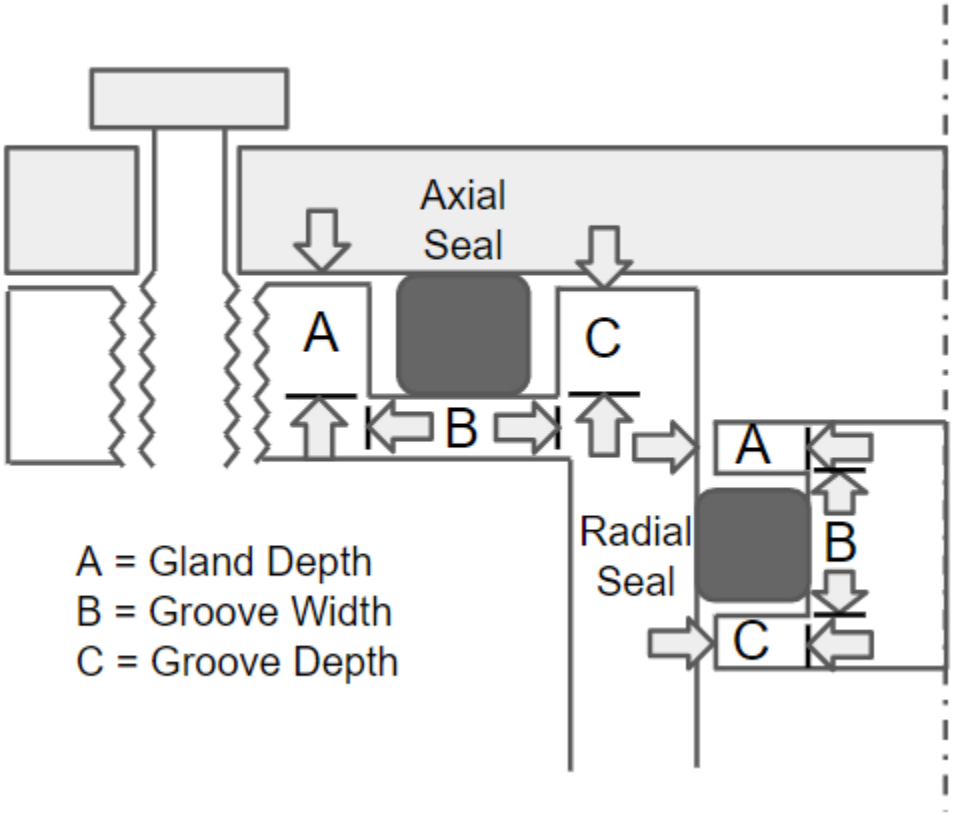

Fig. 5 Key terms for axial and radial seals [24]

At very low temperatures, sealing contact stresses can be lost temporarily as materials reach their glass transition temp or as a result of thermal contraction. Again, these effects can be neglected for this case study given that silicone and ABS are stable at -40°*C*, which is the lower temperature limit for portable speaker usage. The surfaces to be sealed will be made from injection molded ABS, selected for its cost effectiveness and durability. The geometry of the ABS parts is governed by the speaker product requirements.

CHAPTER FOUR: GASKET SEALING SIMULATION

To model the sealing system, only the plastic mating parts and the elastomeric gasket are considered in this study. While there are other parts in the speaker assembly, the loads they impart are assumed to be negligible. Three plastic parts are considered as shown in Fig. 6a, namely the passive frame, driver frame, and housing. Sandwiched between these parts are rubber gaskets of undefined geometry. These rubber gaskets form a closed loop like an O-ring gasket but their cross section may not necessarily be circular. By compressing the gasket and creating contact pressure, a physical barrier is created to prevent water from entering the product housing. Steel wires are threaded to keep the frames joined to the housing (Fig. 6b), but their role can be modeled with a remote-displacement constraint, as will be discussed later, rather than importing the wire geometry into the model. Minor features in the CAD were removed to simplify the simulation model, for a cleaner mesh. Symmetry was also used to reduce the model to a quarter of the actual size of the assembly.

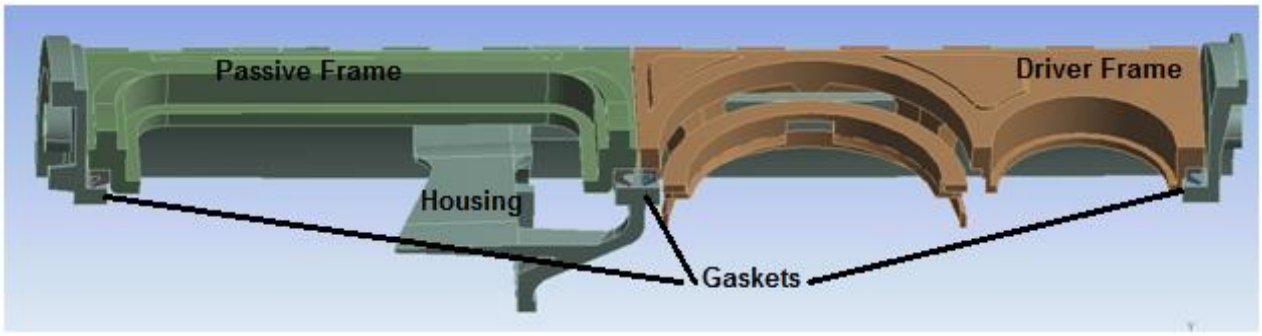

(a) Names of parts used in simulation

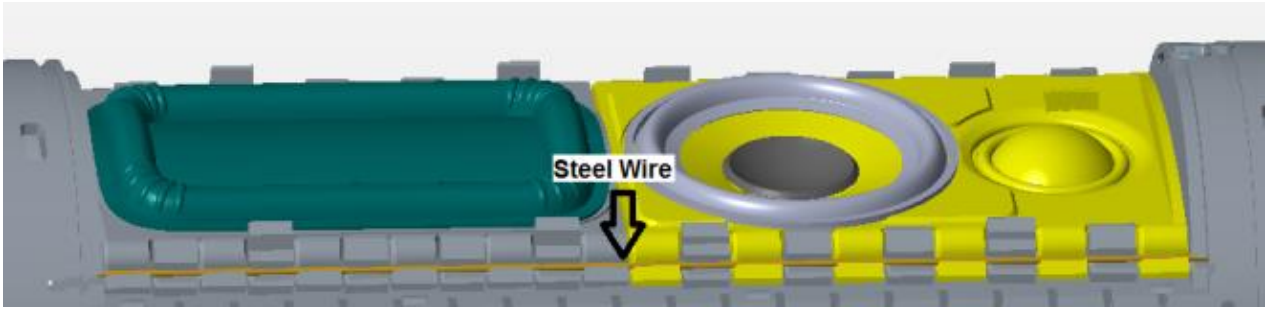

(b) Steel wire connects the frames to housing

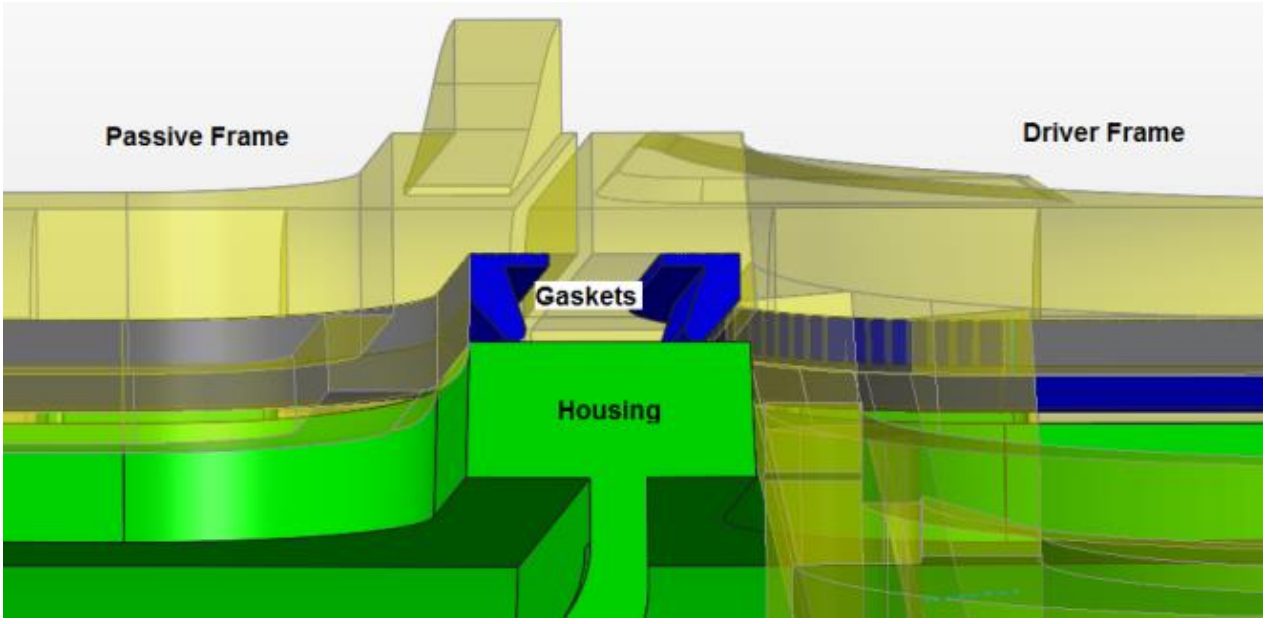

(c) The gap that the gasket must seal

Fig. 6. Geometry used in simulation

4.1 Material constitutive behavior

To develop the material models, material properties for all parts are needed. If material properties are not publicly available from manufacturers, then a lab testing service must be used. The material properties used in this simulation work came from lab testing. The lab measured the properties of the silicone, including the stress-strain response in tension, compression, shear, and the volumetric compressibility. The simulation software used is ANSYS. Typically, lab measurement data values will be input into simulation software, and the software can generate model curve fits. These mathematical models are approximations of the real world response, which are then used to numerically solve for deformations, stresses, and strains. A hyperelastic model was used to model the silicone gasket. Hyperelastic models typically model elastomers well. The constitutive hyperelastic model is defined by a strain energy function, which can take many forms [26]. The Mooney-Rivlin 3-coefficient model was used because it provided a reasonable curve fit (Fig. 7).

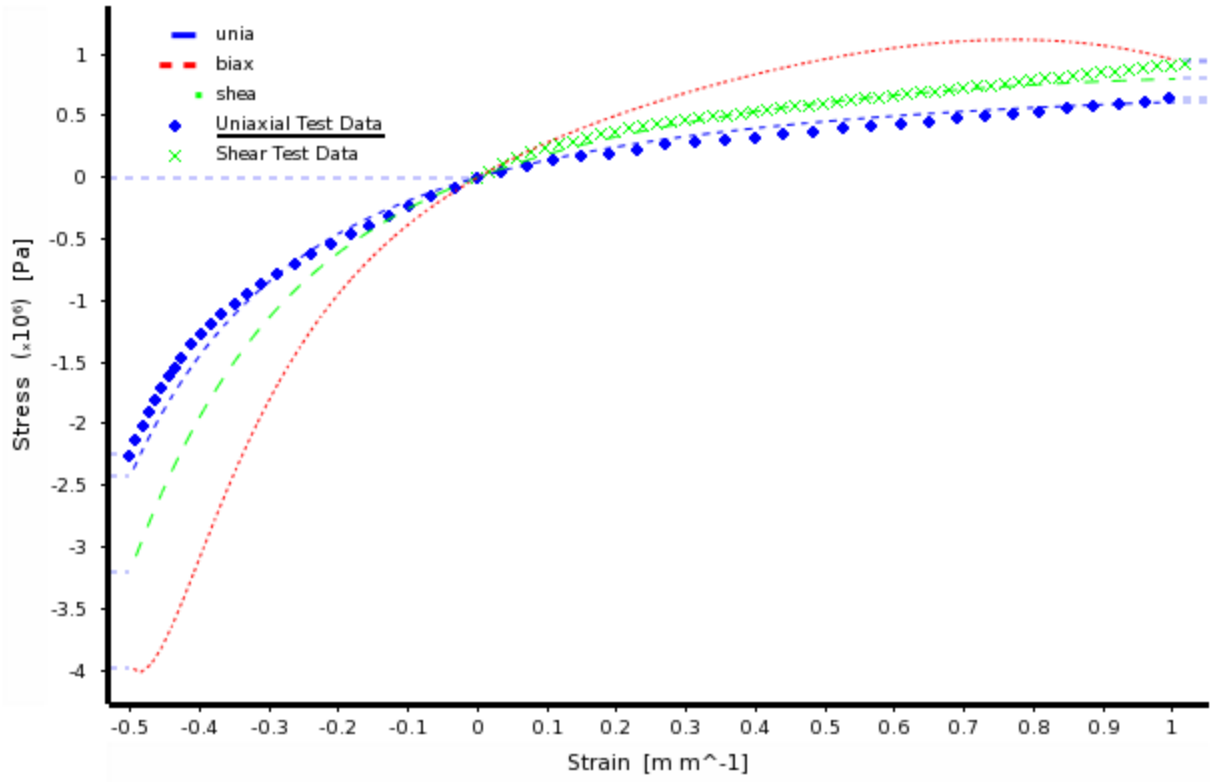

Fig. 7. Silicone material test data and Mooney Rivlin curve fit

The material constants from the curve fit are C_{10}=136460 *Pa*, C_{01}=133240 *Pa*, C_{11}=-12640 *Pa*, and d=0.003 MPa^{-1}.

The following equations are provided to the reader as background [26]. The three-term Mooney-Rivlin model is similar to the polynomial form when $N = 2$ and $C_{20} = C_{02} = 0$

$$W = C_{10}(\bar{I}_1-3)+ C_{01}(\bar{I}_2-3)+ C_{11}(\bar{I}_1-3)(\bar{I}_2-3)+(J-1)^2/d \quad (1)$$

where W is the strain energy potential, $\bar{I}$ are strain invariants and J is the volume ratio. The polynomial form is based on the first and second strain invariants. It is a phenomenological model of the form

$$W = \sum_{i+j=1}^{N} C_{ij}(\bar{I}_1-3)^i(\bar{I}_2-3)^j + \sum_{k=1}^{N}(J-1)^{2k}/d_k \quad (2)$$

where the initial bulk modulus K and initial shear modulus μ are

$$K_0 = 2/d_1 \quad (3)$$

$$\mu_0 = 2(C_{10} + C_{01}) \quad (4)$$

The three strain invariants are commonly used to define the strain energy density function.

$$I_1 = \lambda_1^2 + \lambda_2^2 + \lambda_3^2 \quad (5)$$

$$I_2 = \lambda_1^2 \lambda_2^2 + \lambda_2^2 \lambda_3^2 + \lambda_3^2 \lambda_1^2 \quad (6)$$

$$I_1 = \lambda_1^2 \lambda_2^2 \lambda_3^2 \quad (7)$$

The stretch ratio (or simply 'stretch') λ is defined as

$$\lambda = L/Lo = (L_0 + \Delta u)/L_0 = 1 + \varepsilon_E \quad (8)$$

The volume ratio J can be defined as

$$J = \lambda_1 \lambda_2 \lambda_3 = V/V_0 \quad (9)$$

As shown above, J can be thought of as the ratio of deformed to undeformed volume of the material.

An isotropic linear model is used to represent the ABS plastic parts with Young's modulus = 2.4 G*Pa* and Poisson's ratio = 0.35. A modified-time-hardening creep model was added to the ABS material model and creep strain ε_{cr} is defined as

$$\varepsilon_{cr} = (C_1 \sigma^{C_2} t^{C_3+1} e^{-C_4/T})/(C_3 + 1) \quad (10)$$

The dependency of creep deformation on stress σ, strain ε, time t, temperature T are generally modeled with a form similar to the following [26]:

$$\dot{\varepsilon}_{cr} = f_1(\sigma)\, f_2(\varepsilon)\, f_3(t)\, f_4(T) \quad (11)$$

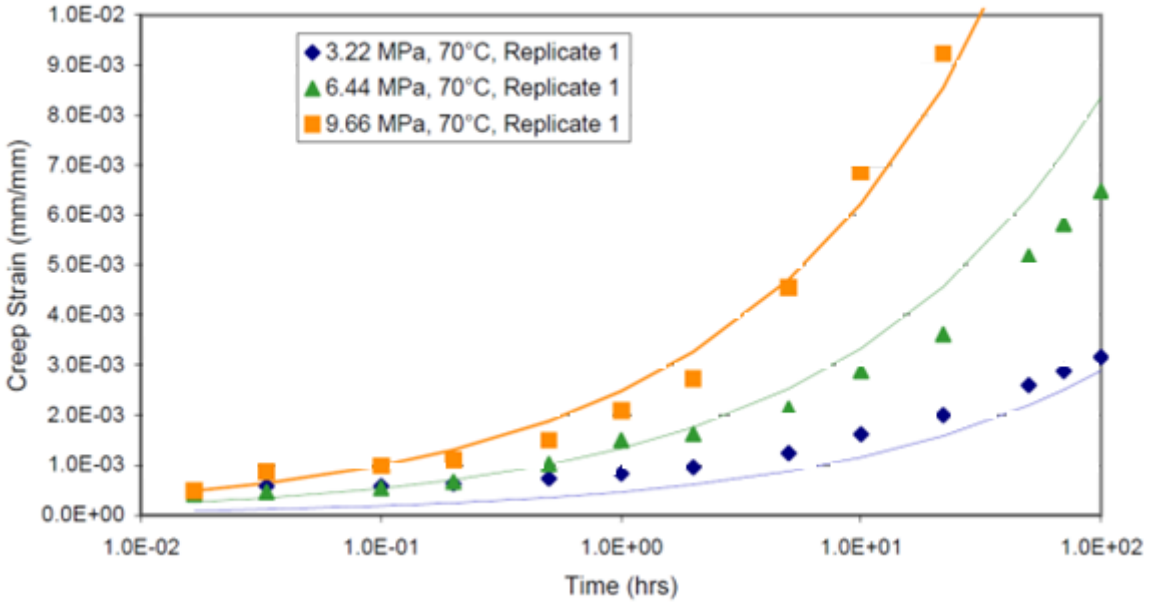

Fig. 8. ABS creep data and curve fit

Creep data was gathered both from lab testing and from online material databases. The modified-time-hardening creep model was selected because the available creep data could be input into the equation directly. The measured parameters are stress, strain, time, and temperature. The curve fitting is done in ANSYS Mechanical APDL. It is worth mentioning that due to the sparsity of data points and the relative simplicity of creep mathematical models, the curve fits developed are rough approximations. Fig. 8 shows a sample curve fit provided by the testing lab. Notice how the 3.22M*Pa* data points do not match very well with the curve fit line.

The solved creep constants are shown below in Table 2. There are 4 sets of constants for 4 different temperature conditions. The ANSYS software uses interpolation when computing creep behavior at temperatures between 23 and 80°*C*.

Table 2. ABS creep constants

Temperature ($°C$)	Creep Constant 1	Creep Constant 2	Creep Constant 3	Creep Constant 4
23	1.2607E-16	1.5842	-0.71721	0
40	2.6497E-15	1.4046	-0.69276	0
60	5.8262E-14	1.2895	-0.6927	0
80	1.057E-12	1.164	-0.6324	0

Both the hyperelastic model and plastic creep model were tested in simulation to check that the models were working as intended. Basic compression cylinders were modeled in CAD, and stretched and compressed in ANSYS.

4.2 2D Cross-Section Shape Optimization

Due to the computational expense of fully nonlinear 3D structural simulations, simplifications are made when possible to reduce time to solutions. 2D representative models are used for initial study. To develop a few terms, in this study, there are 3 key parameters in action. First, there is the 'compression pressure' which is needed to create sealing. This compression pressure, when applied over a contact area, produces a compression force. This force induces bending of plastic beams, similar to the distributed load on a simply supported beam. The beam bending increases with increasing temperature and a portion of the deformation becomes permanent 'creep strain'. In the midspan of the beam, where the beam deformation is greatest, there exists the greatest potential for sealing failure. There the 'compression height' or amount of linear interference, of the gasket is greatly reduced. Take for example, an O-ring with a cross-sectional diameter of 3*mm* that is compressed in a groove that has a 2*mm* gland depth. The

compression height is then 1*mm* creating a certain compression pressure. This pressure must be sufficiently high to seal, and yet this same pressure induces beam bending and creep, which reduces compression height. With reduced compression comes a gradual decay in the creep strain rate until eventually a steady state is reached.

To develop a concept of sealing margin, imagine a gasket cross-section that is 100*mm* tall and compressed to 1*mm*. While this is 99% compression, imagine that somehow the resulting compression force was very small. Then the creep strain would also be very small. Imagine that somehow the creep strain is only 1*mm*, meaning the sealing surface beam permanently deflects 1*mm*. Then the gasket compression height would only be reduced from 99*mm* to 98*mm*. The gasket is in no danger of sealing failure and therefore has a large "sealing height margin." In this study, the allowable space for the gasket, when compressed, is 2*mm* tall and 3*mm* wide. Suppose a 4*mm* tall gasket is inserted into the space. Then to fit into the 2*mm* gap, the gasket would be compressed 50%. Suppose this amount of compression leads to high compressive forces, high creep strain greater than 2*mm*, and therefore total loss of compression height and pressure, and ultimately sealing failure. Then the gasket has no height margin after temperature-induced creep effects.

What steps can be taken to improve the sealing height margin? Suppose the height of the gasket is increased to 5*mm* tall. Then the initial compression height increases from 2*mm* to 3*mm*. But how much will the creep strain increase with this larger gasket size? Perhaps it will increase the creep strain but the resulting creep strain still remains under 3*mm*. Then at least there would be some compression height remaining so that it would have some height margin. Now suppose instead that the gasket height is reduced to 3*mm*. Then the starting compression height is 1*mm*, the compression force is smaller and the creep strain is smaller. But will the creep strain be under

1*mm* so that there is some compression height margin leftover? In this case study, simulation is used to study many cross-section shapes to understand the relationship between the parameters.

A rectangular cross section was first studied. As the width of the rectangle increased, the resulting compression force increased in proportion because the contact surface area increased. This higher compression force leads to higher creep strain and is undesirable. Conversely, a smaller width rectangle lead to lower compression forces due to smaller contact surface area. This effect is highly desirable but care must be taken not to make the contact surface too narrow. The presence of particle contaminants, scratches, or surface roughness can defeat seals with too narrow of contact surface. The minimum safe contact width will be assumed to be 0.5*mm* for this study. However, this does not mean that the gasket body width can be 0.5*mm* because such a narrow cross-section would be prone to buckling as the gasket is compressed, leading to erratic displacement of the gasket. The gasket must be stable during assembly and in the assembled state, and resistant to vibrations or shock loading during the life of the product.

Next it was observed that a 4*mm* tall gasket compressed into a 2*mm* gap exerted the same compression pressure as a 3*mm* tall gasket compressed into a 1.5*mm* gap. Compression pressure is proportional to the compression strain % as seen in Fig. 9. The compression strain in this example is 0.5 or 50% compression. The 4*mm* tall gasket exerted the same pressure as the 3*mm* tall gasket but has a better initial compression height value of 2*mm* vs 1.5*mm*, meaning it will have better height margin after creep.

These two observations have suggested that tall and narrow gaskets are desirable and serve to narrow the focus for shape optimization. It would be far too computationally expensive to study the vast number of gasket shapes imaginable. In regard to material hardness, it became evident that softer gasket materials would lead to lower creep strain and greater height margin

after creep effects. The silicone hardness that will be evaluated are Shore 30A, 40A, 50A, and 60A.

The next step was to consider the stress-strain curve. As a square gasket is being compressed, the force rises gradually and then begins to grow exponentially. Suppose a gasket starts at 50% compression. After creep effects take place, there may only be 10% compressive strain leftover, or even 0% compressive strain. Indeed, many square gaskets and circular gaskets had been trialed experimentally and all had led to sealing failure.

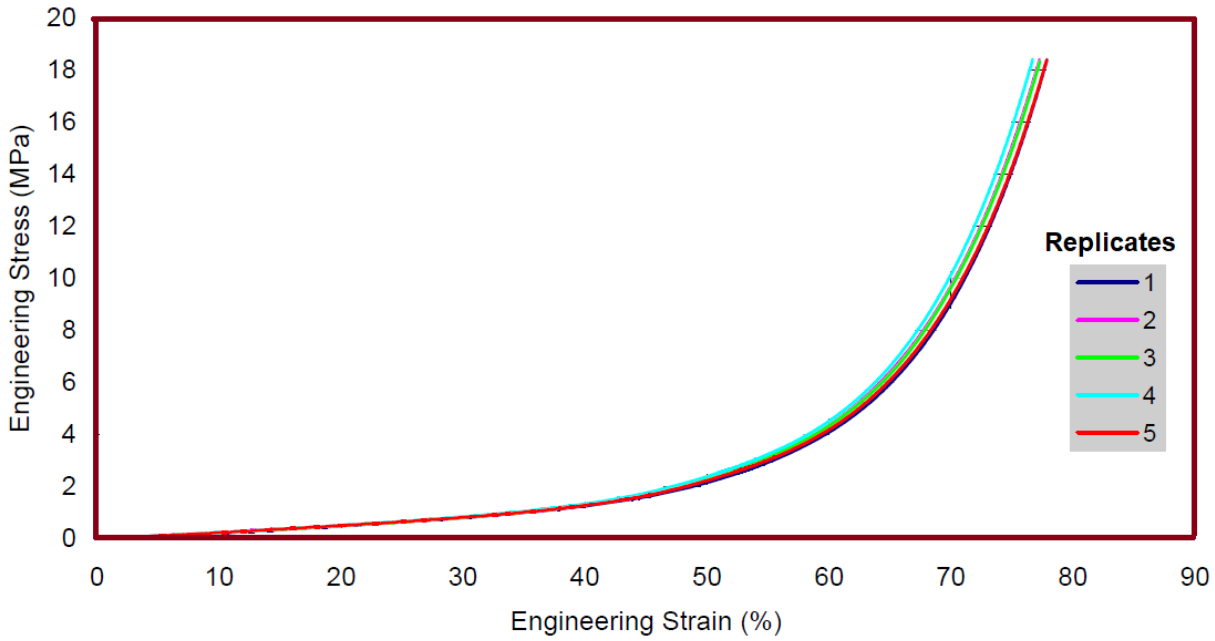

Fig. 9. Engineering stress-strain curve for Silicone Rubber Shore 40A, 5 replicates

It became clear that what is needed is a gasket with a force-compression curve that is very flat, where the curve is just above the sealing pressure target and remains flat even as the gasket is compressed further and further. In this way, the gasket can have the most initial compression height, and yet the creep will be minimized, and therefore the height margin will be maximized.

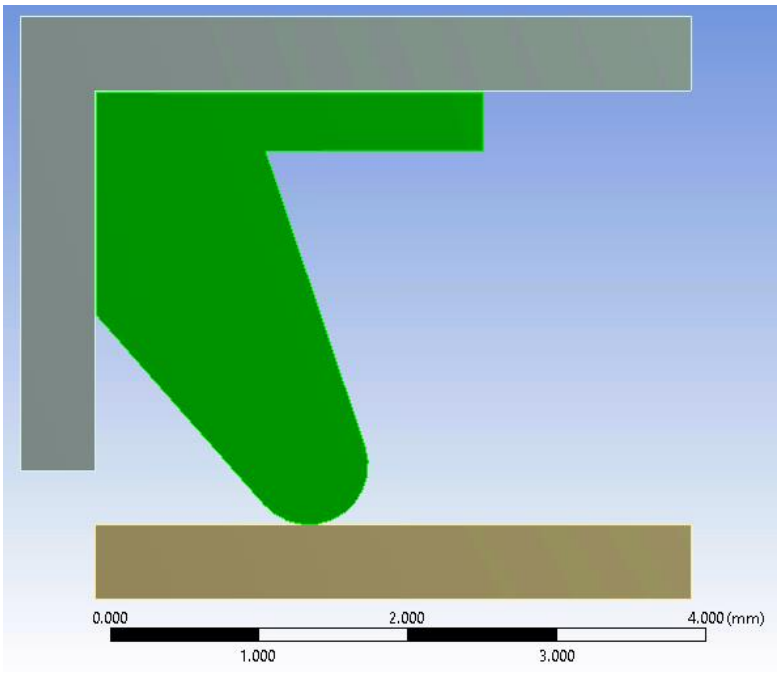

Fig. 10. Gasket seal cross section

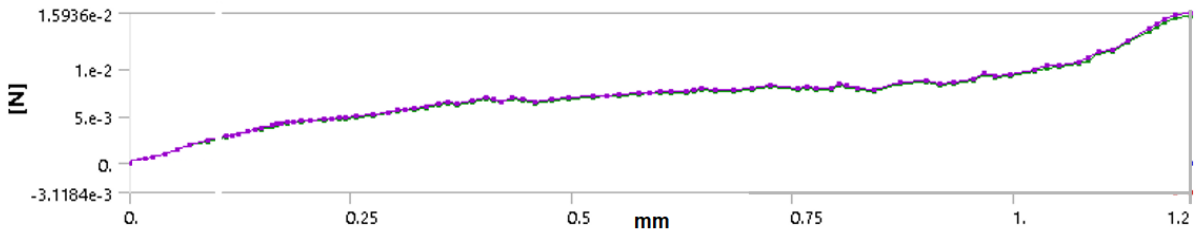

Fig. 11. Force (*N*) vs compression (*mm*) curve of 2D gasket in Fig. 10

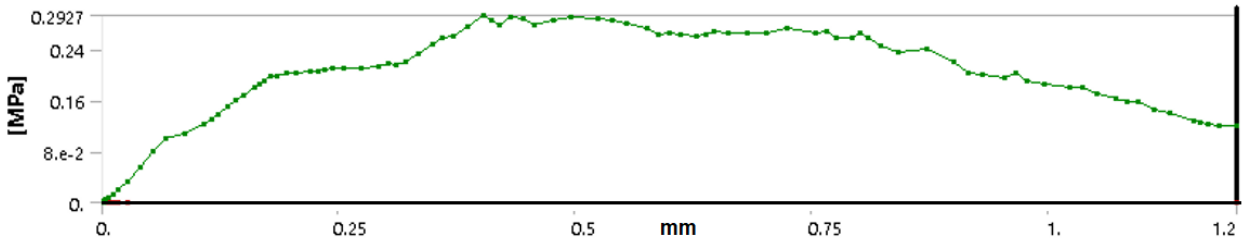

Fig. 12. Pressure (M*Pa*) vs compression (*mm*) curve of 2D gasket in Fig. 10

After many simulation trials, the best performing cross sectional shape was selected and it is shown in Fig. 10. The force-compression curve is flat and low in Fig. 11. The pressure-compression curve is sufficiently higher than the hydrostatic pressure of 0.01M*Pa* in Fig. 12. This gasket shape has a designed compression height of 1.2*mm*, starting from 2.9*mm* tall and compressed into a 1.7*mm* gap. From the graph, so long as the creep strain doesn't exceed 1.1*mm*, there should be sufficient sealing pressure leftover.

For the 2D simulation, the materials used are silicone rubber and structural steel. At this stage, the flexibility of the sealing surfaces is not yet considered. The upper surface of the gasket is bonded to the top sealing surface, representing a glue bond, as shown in Fig. 13. All other surfaces of the gasket have a frictional contact definition with the steel surfaces. The upper steel part is fixed while the lower steel part is brought up 1.2*mm* to study the force-compression response.

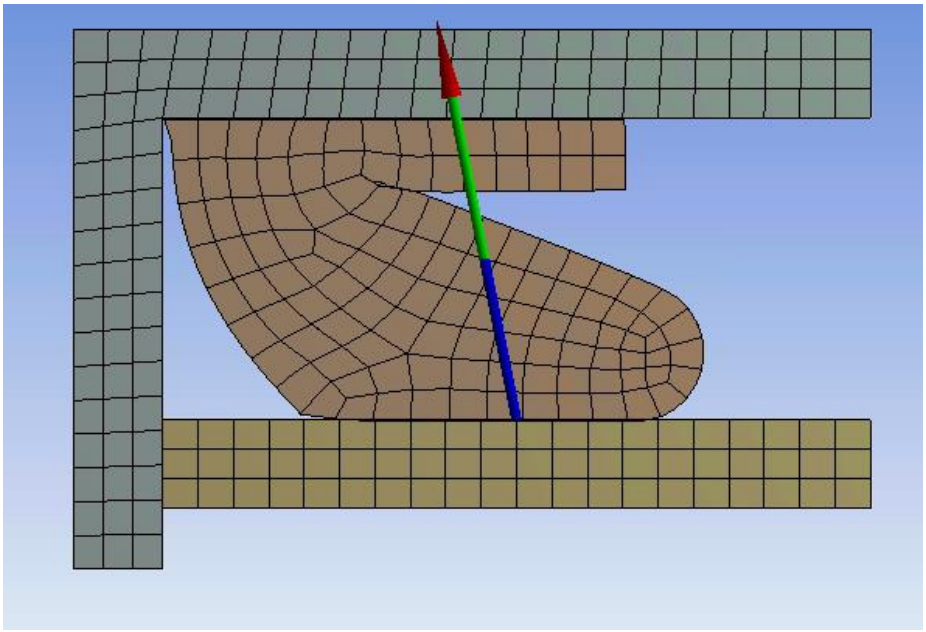

Fig. 13. Gasket seal cross section compressed with force reaction arrow

During compression, the gasket folds and slides, providing consistent sealing force that only slowly increases. The dimensions were optimized by varying the key parameters in increments of 0.1*mm*, highlighted in red below in Fig. 14.

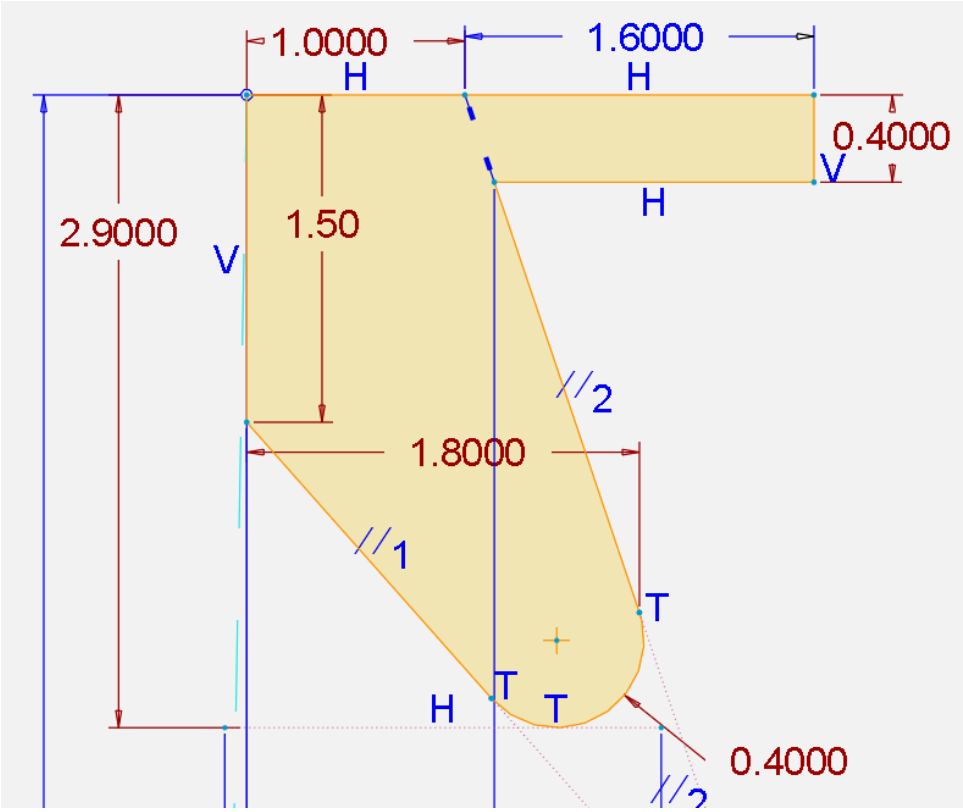

Fig. 14. Gasket seal cross section with key parameters highlighted in red

The parameter combinations studied were not completely exhaustive. Instead, after ~100 parameter combinations were simulated, the best performing combination was selected for the next stage of simulation. This gasket shape has the advantage of self seating, that is, the compression forces tend to push the gasket into the secure corner of the driver and passive frames.

4.3 3D Model Setup

There are five 3D bodies in the simulation (Fig. 15). The housing, driver and passive frames are given an ABS material assignment. The driver and passive gaskets are given a silicone rubber assignment. The 3D gasket shape is formed by sweeping the 2D cross-section along the perimeter of each frame.

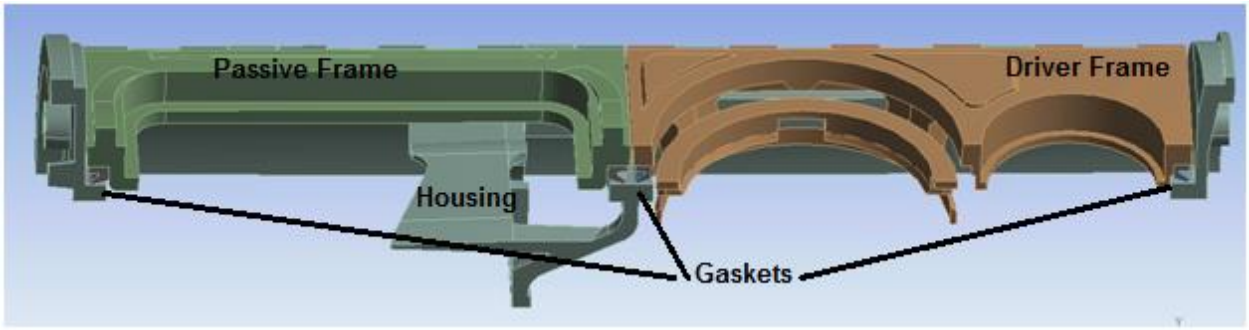

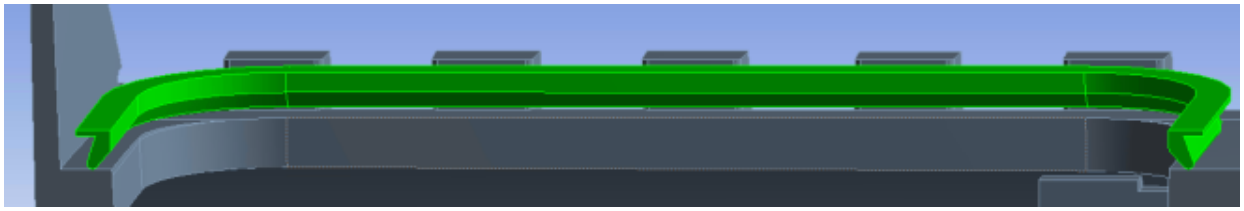

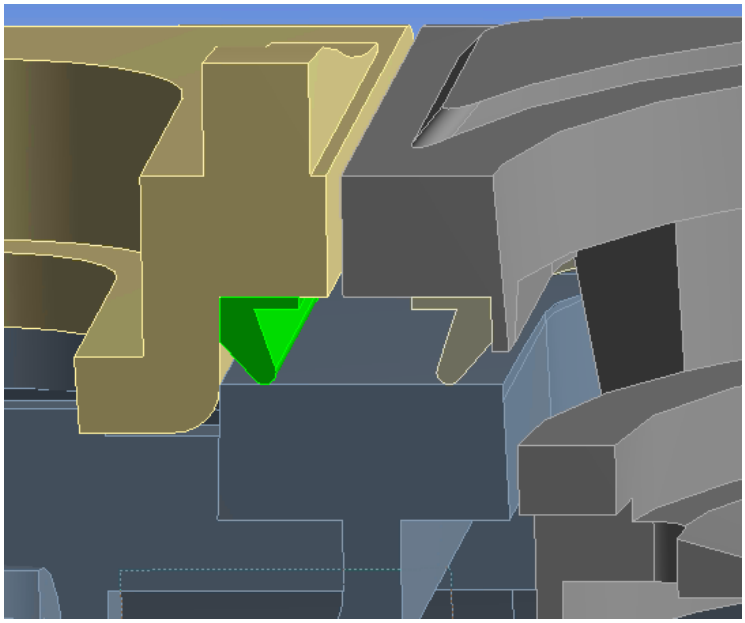

Fig. 15. Geometry used in simulation

As with the 2D simulation, the gasket's top surface is bonded to each frame. The rest of the gasket surfaces are given a frictional contact definition. A friction coefficient of 0.2 was found to produce the correct folding behavior. During folding, the gaskets surfaces may experience self-contact, so that contact is also defined for the simulation.

For meshing, hex dominant method was used to model the ABS parts with a mesh size of 1.0mm. The housing surface that contacts the gasket had mesh sizing of 0.5mm to improve convergence. The gasket bodies were meshed with the sweep method using hex elements, sized at 0.2mm.

To properly constrain the model, a fixed support is applied at surface-A of the housing. Frictionless supports are used on the symmetry surfaces of all parts (Fig. 16). The load steps of the analysis compress the gasket, assembling the gasket in the same manner as on the assembly line. Remote displacements are used to move the frames towards the housing, compressing the gaskets. The remote displacements allow freedom of rotation at the sides of the frames, mimicking the behavior of the steel wires mentioned previously. The steel wires fix the frames to the towers on the housing but they allow for rotation around the axis of the wire. It can be visualized as a pin joint.

Then the entire assembly is exposed to elevated temperatures for a set period of time. A thermal condition is imposed on the ABS parts, allowing the temperature to be set to 70°C and creep effects are turned on. In this step, creep strain develops in the ABS frames and housing. After the simulation is finished solving, the contact pressures before and after thermal exposure are examined.

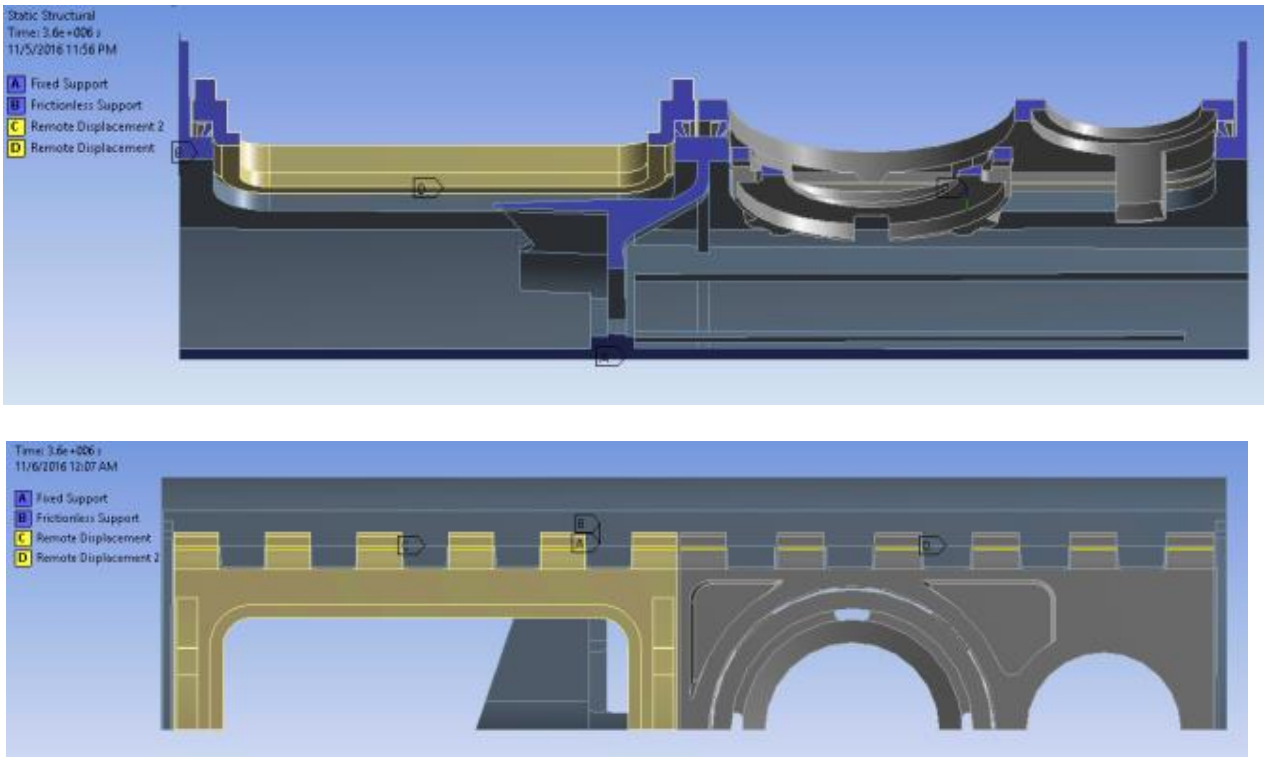

Fig. 16. Simulation constraints

Under the solutions branch, the directional deformations at various time points are requested. The direction of interest is in-line with the compression height dimension. Also of interest are the contact pressures at various time points and the force reaction of assembling the driver and passive frames at time zero, before heat exposure. These force reactions will be used to validate the simulation model experimentally.

4.4 Simulation Results

The optimized gasket sealed with a minimum pressure of 0.10 M*Pa* before thermal relaxation and a minimum of 0.08 M*Pa* after 120 hours of exposure to elevated temperatures (Fig. 17). 120Hrs is used because this was later found to correlate well with the steady state

creep value. These sealing pressures are measured in the midspan of the center beam of the housing, the known weakest sealing point.

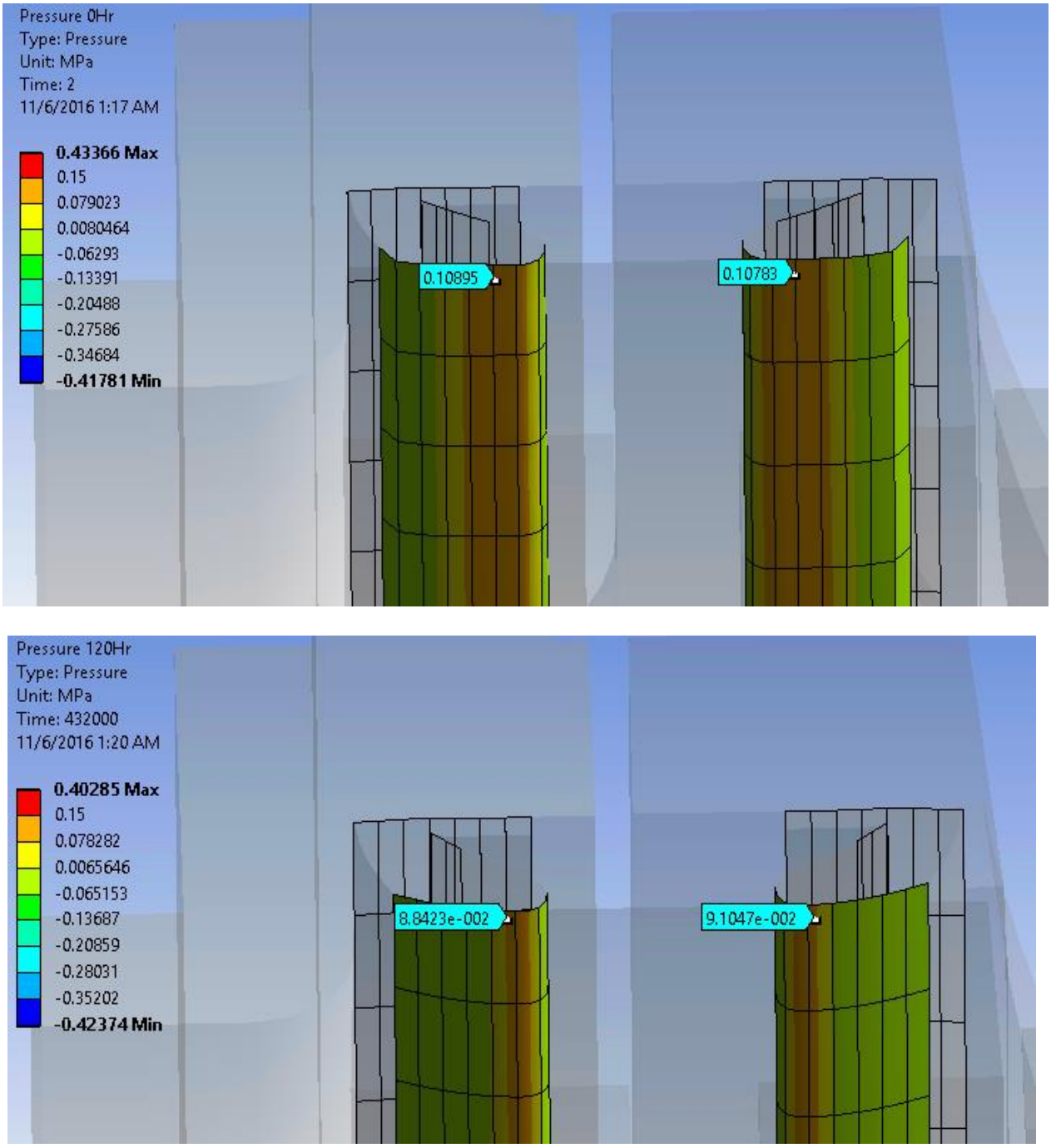

Fig. 17. Compression pressures before and after thermal creep effects

The assembly force for the passive gasket was only 36*N* while the driver gasket assembled at 50*N* using Shore 40A hardness gasket. The amount of thermal creep measured to be 0.4*mm* (Fig. 18) along the direction of gasket compression, meaning there would be 0.7*mm* of height margin after creep, assuming the initial height margin is 1.1*mm* but this value must be verified.

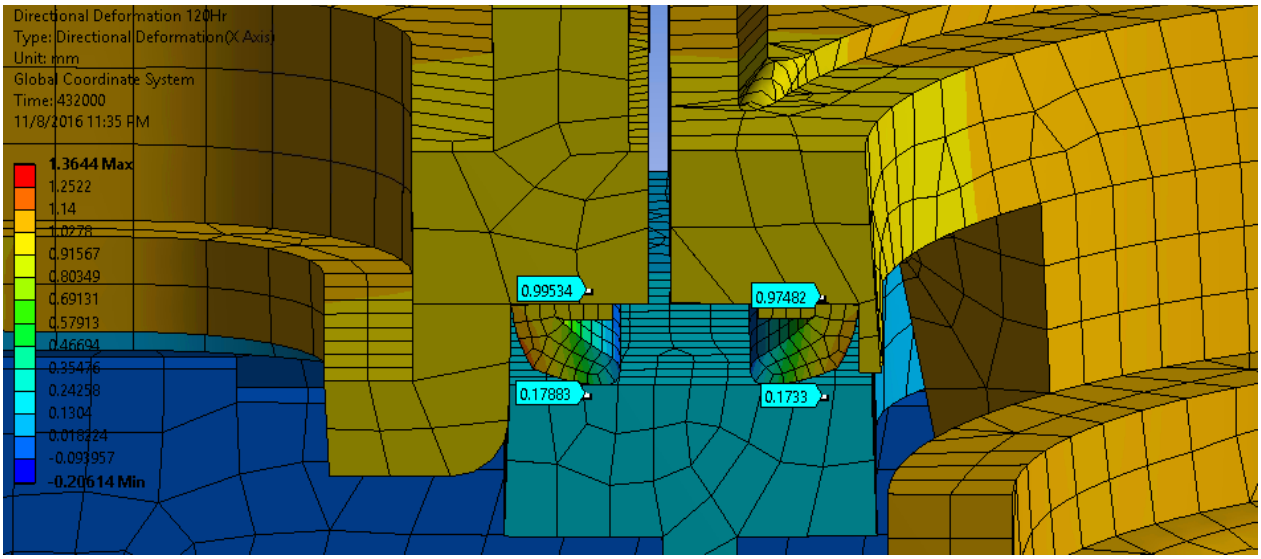

Fig. 18. Directional deformation of frames and housing. Note that the frames are brought down 1.21*mm* to compress the gasket, before relaxing to the 0.99*mm* displacement height, creeping 0.22*mm* upward. The total creep between the two ABS parts in this image is then 0.22 + 0.18 = 0.4*mm*.

4.5 Air Sealing Consideration

Due to the shape of the gasket, water pressure acting on the external face of the gasket tends to increase sealing pressure against the housing and frame (Fig. 19). This means that in theory, the gasket design could withstand water pressure much greater than the IPX7

requirement. In fact, it should seal against any amount of water pressure up to the point where the gasket is extruded or dislocated.

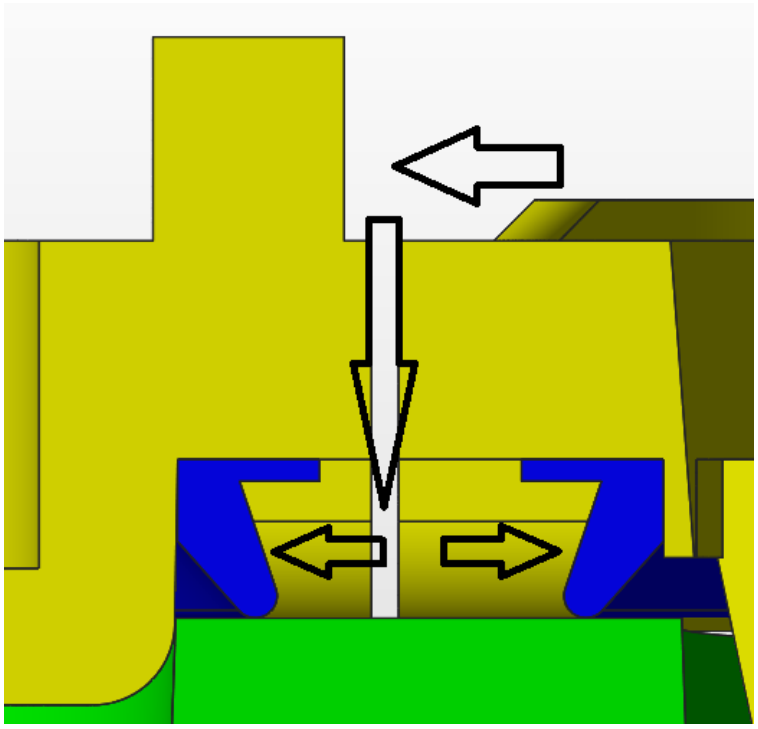

Fig. 19. External water pressure acting on the external gasket surfaces

On the other hand, air pressure acting on the internal face of the gasket tends to lessen sealing pressure. Internal pressure could defeat the gasket sealing pressure, and create an air leak while the speaker is playing music. Because an air leak would lead to sound distortions, this places another constraint on the acceptable sealing pressure. Because of this requirement, the initial height margin is experimentally found to be 0.8*mm*. While the external water sealing margin may be 1.1*mm*, after considering the internal air sealing requirement, the sealing margin is only 0.8*mm*, the lower of the two values. Given the creep value of 0.4*mm* obtained previously,

and the fact that assembly of parts tolerances is +/- 0.2*mm*, this means the final height margin could be as low as 0.8-0.4-0.2 = 0.2*mm*. More margin would be beneficial.

Since the gasket is believed to be well optimized, minor changes were made to the frames and housing to lessen the creep. This was done by stiffening the structure with more ABS material, prioritizing increasing the height of the beams over other dimensions, since height has the greatest impact on stiffness. However, there are spatial limits that restrict the frames and housing from becoming abundantly stiff. There are also molding defect, such as sink marks, that can result if regions of a molded part are too thick. Therefore, the frame and housing can only be stiffened so much.

Another idea for sealing improvement was to add a ramp of material on the housing (Fig. 20). The ramp would have added 0.5*mm* of thickness to the midspan of each beam. The idea was to locally increase the compression of the gasket in the midspan of the beams. In doing so the initial height margin would have increased by 0.5*mm*. The extra plastic would compensate for the fact that the midspan of each beam sags from thermal creep effects.

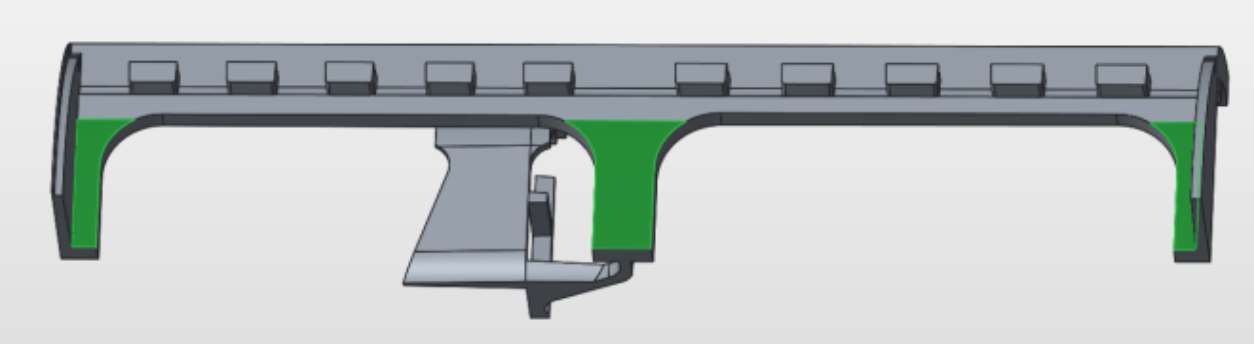

Fig. 20. Highlighted in green are locations where material could have been added to the housing, ramping the flat surface to be 0.5*mm* higher in the midspan of each beam

This increased compression carries a trade-off which is that the creep strain in the midspan of the beam also increases. However, because simulation shows the creep strain only increases by an additional 0.25*mm* (Fig. 21), there is a net gain of 0.25*mm* for the final height margin, for a total of 0.45*mm* final height margin. Such a margin would guarantee reliable sealing performance for 100% of production units. It was later determined that this improvement was not needed.

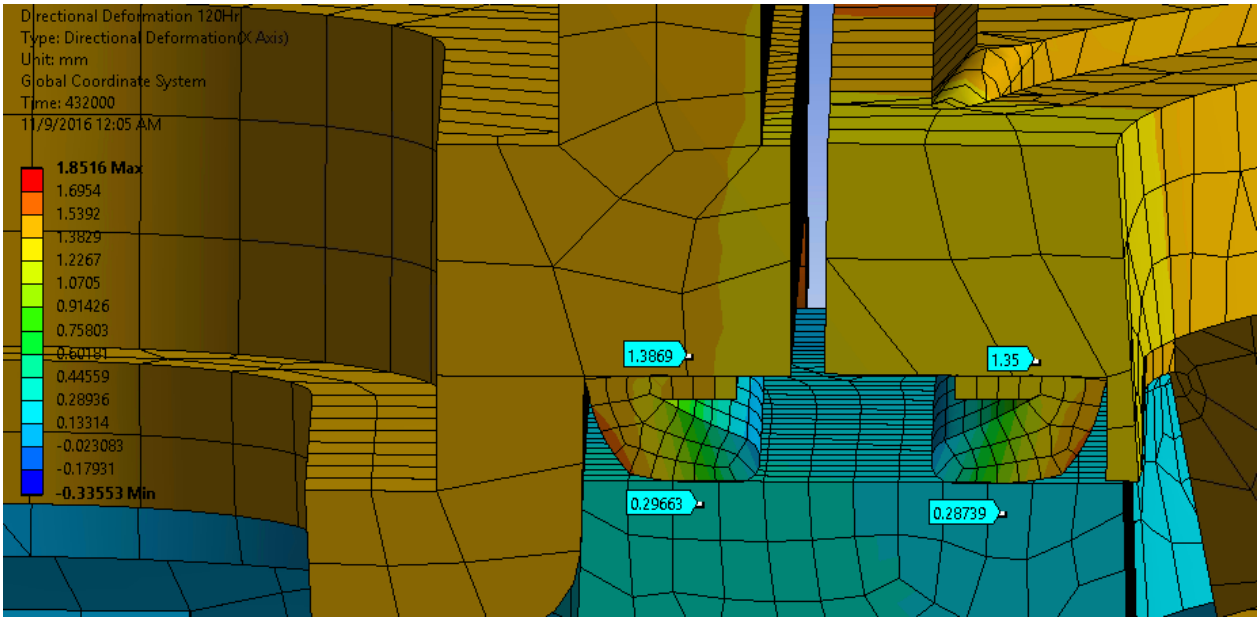

Fig. 21. Increased creep strain at midspan of center beam

CHAPTER FIVE: EXPERIMENTAL VERIFICATION AND TESTING

Silicone gaskets were obtained from a Chinese supplier in shore hardness of 30A, 40A, 50A, and 60A. This range of hardness would allow greater data collection and more sealing options. Real frames in the ABS material were also obtained. Housing fixtures were 3D printed out of Vero Gray material which has similar stiffness to ABS. The black frame, yellow gasket, gray housing, and silver steel wires are shown in Fig. 22.

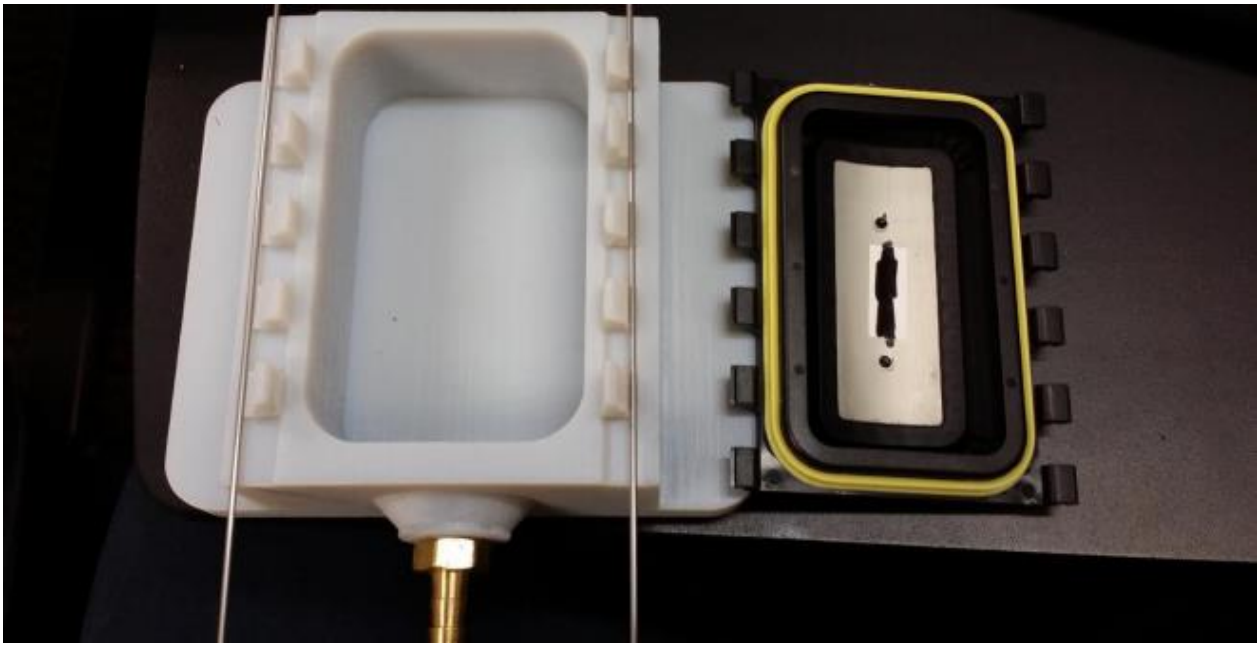

Fig. 22. Test fixture for experimental validation

In the images below, note that the deformation of the gasket is similar between simulation and real world (Fig. 23).

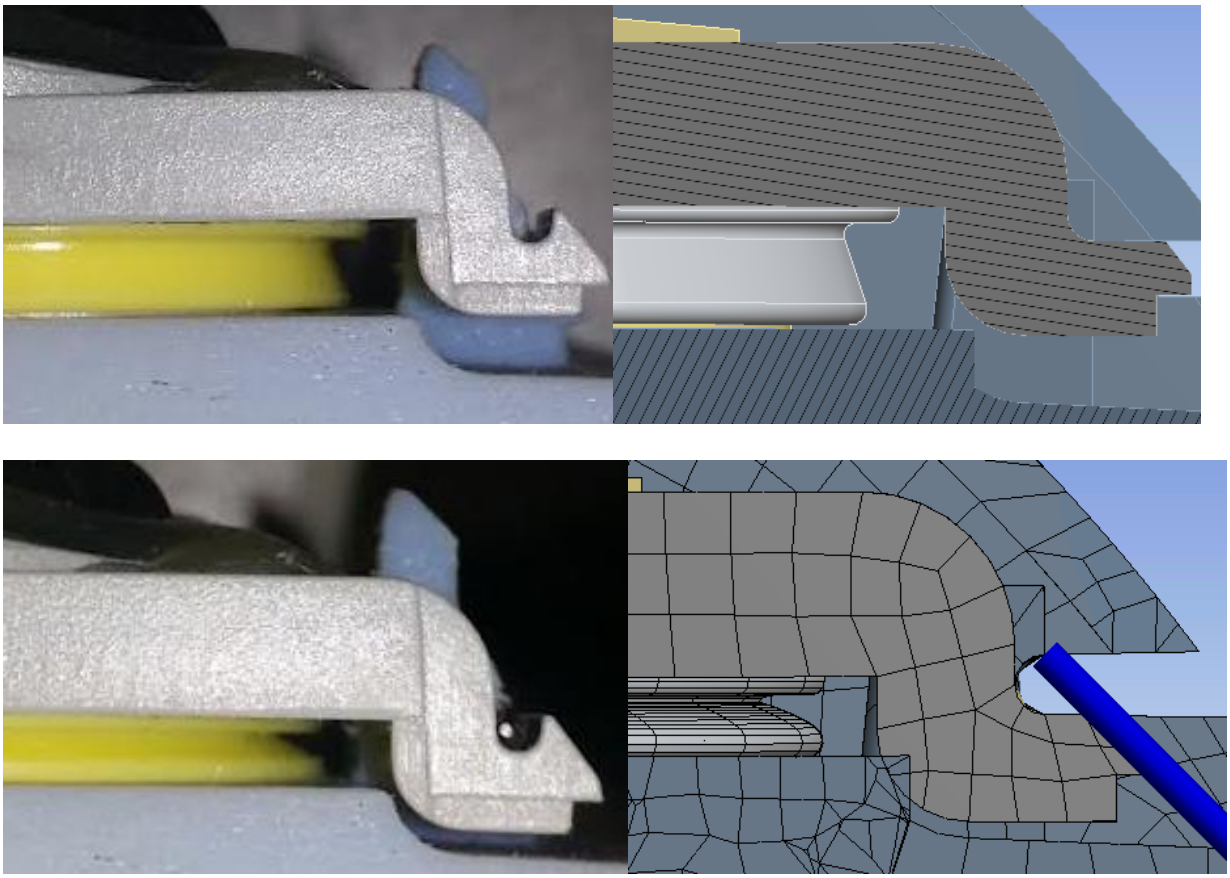

Fig. 23. Gasket assembly before and after compression

Using a Zwick Roell uniaxial force-displacement measurement machine, gaskets were compressed between housing and frame. During compression, force reactions were recorded as a function of displacement or travel of the Zwick load cell sensor. Measuring the passive gasket compression gave the following force curves.

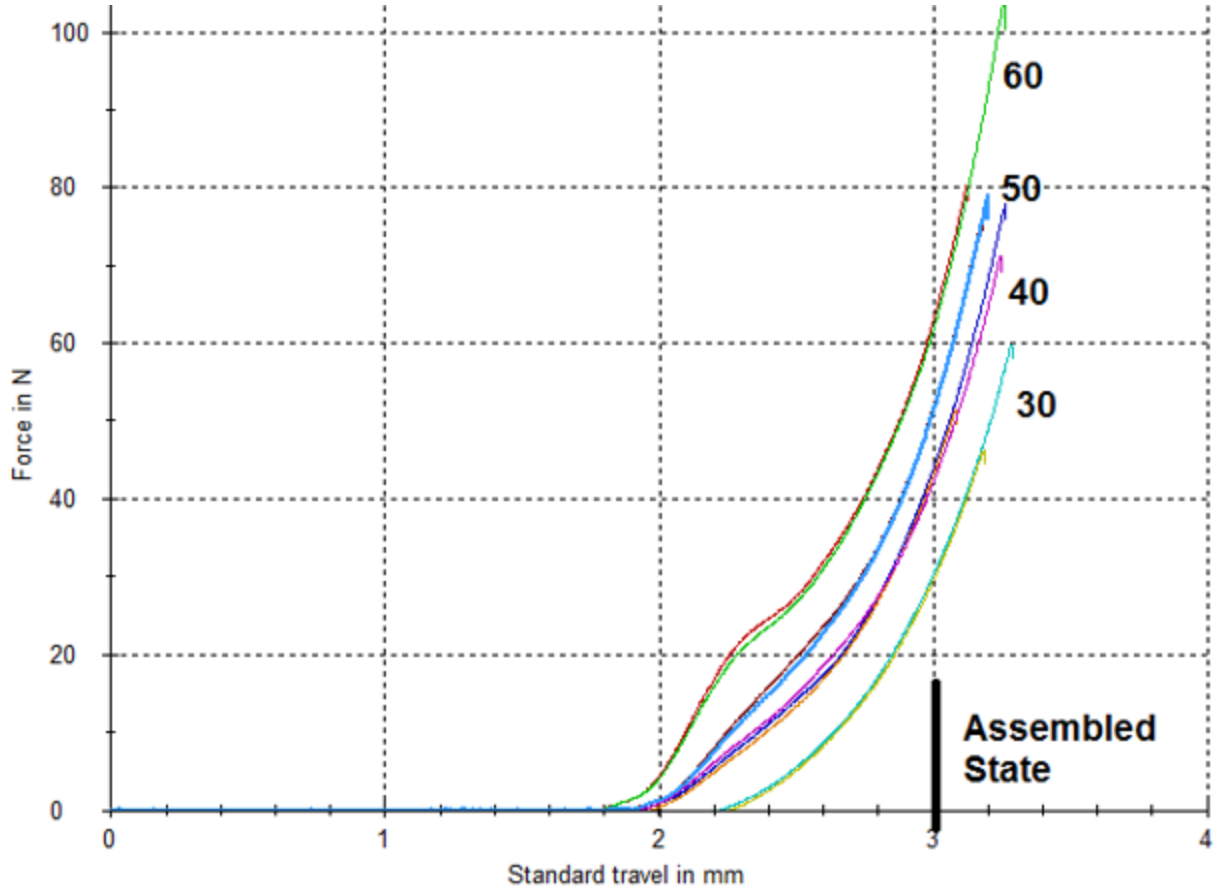

Fig. 24. Passive gasket force curves, comparison among various hardnesses

In the graph, the load cell travel has been calibrated such that when the load cell has traveled 3mm, the gasket is in its assembled compression state. For the Shore 30A gasket, the force reaction is about 30*N*. For the Shore 40A gasket, the force reaction is about 40*N*. For the shore 50A gasket, the force reaction is about 50N. For the shore 60A gasket, the force reaction is about 60*N*. The force reactions for the Shore 30A and 40A match up well with simulation, within 20%. In the 60A force curve, there is a visible bump in the graph, indicative of static friction buildup that eventually turns into kinetic friction as the gasket slides. The force-displacement

curve simulated in the 2D analysis also displayed this bump, which confirms that the friction coefficient of 0.2 is appropriately capturing real world behavior.

In the 30A force curve, compression begins at the 2.2*mm* mark, while all gaskets should start compression at 1.8*mm* per the design. This indicates that the 30A gasket is not returning to its uncompressed state between load measurements. The gasket is too soft to rebound quickly. For this reason, the next softest gasket is favored, namely 40A.

Similar measurements were taken for the driver gasket (Fig. 25). Since both gaskets use the same cross section, the shapes of the force curves are also similar. With the force reactions verified, the contact width is checked next. Clear acrylic blocks were machined for this verification. When the blocks are used to compress the silicone gaskets, the color in the compressed regions darken. Note the similarity of the darkened contact surface seen on real parts and the contact surface predicted by simulation (Fig. 26). When predicted force and area values match reality, contact pressures also match reality.

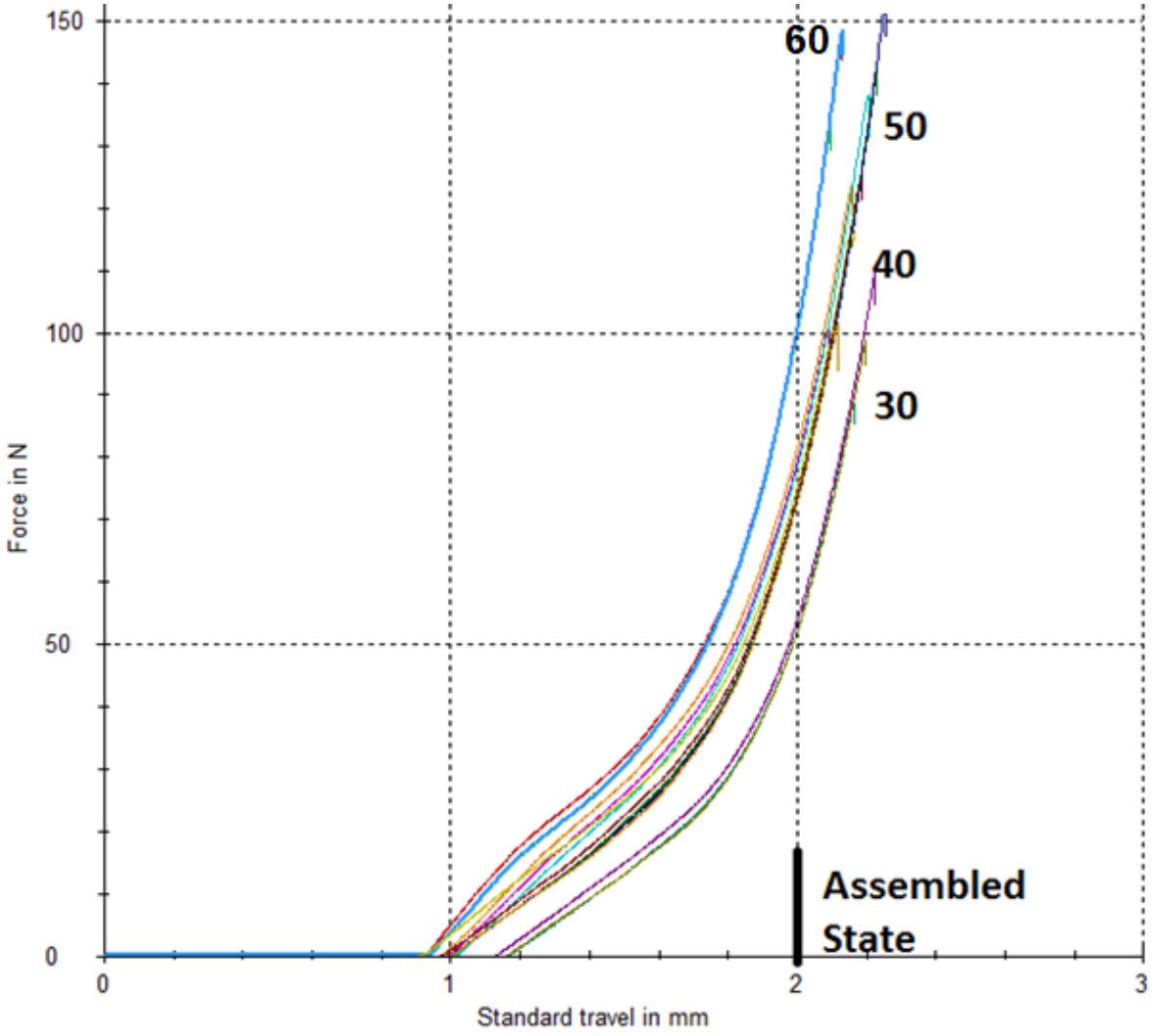

Fig. 25. Driver gasket force curves, comparison among various hardnesses

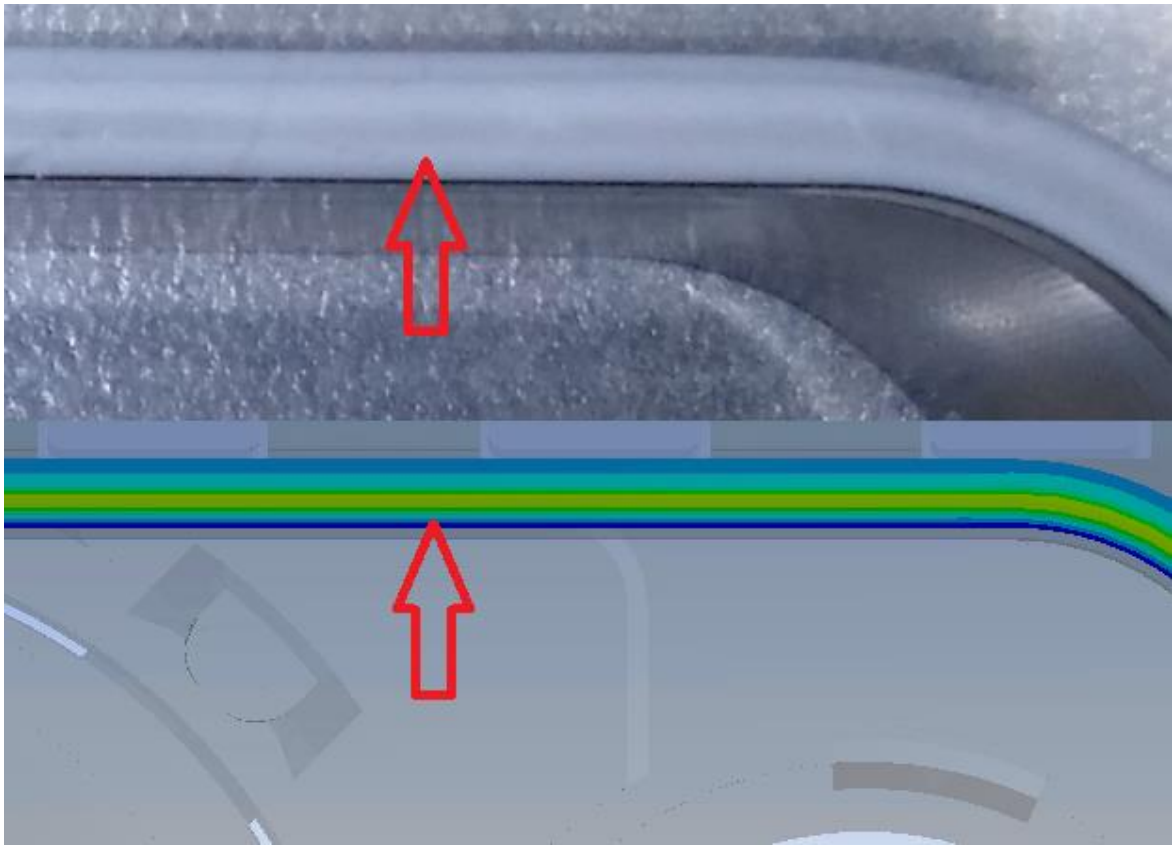

Fig. 26. Compression surface bands, real (top, gray band) and simulated (bottom, green band)

The next verification was gasket sealing performance using pressurized air. The printed housing test fixtures have the shape of a fully enclosed box, except for the opening on the top face where the gasket wraps around, and an opening for a brass hose fitting. Refer to Fig. 27. The hose fitting is connected to a pressure source that is kept at a constant 0.5 *psi* or 0.00345 M*Pa*. Why 0.5 *psi*? It represents the maximum dynamic air pressure that will be generated by this speaker. In between the housing and pressure source, a flow meter measures the flow of air (Fig. 27).

Fig. 27. Flowmeter to measure air leaking past the gasket. Units are in *ccm*.

Any leaks in the housing-frame-gasket system would drop the pressure in the housing air volume. Then the pressure source would replenish the housing pressure, by diffusion mechanism, causing air to flow. In this way, the leak rate of the seal system can be measured. Testing showed that air flowrates through the gasket seal measured below 1*ccm* for all Shore hardness tested but was noticeably higher for the Shore 30A. This is another reason why 40A is favored over 30A.

When the housing fixture is placed under water, the flowrate dropped below 0.5*ccm*. This is expected since water pressure will tend to augment compression forces as discussed earlier. When the housing internal air volume was placed into a 0.5 *psi* vacuum pressure state, the airflow rate was below 0.5*ccm*. Again, this is because internal vacuum pressure augments compression forces. These measurements applied to all shore hardness tested and to both passive and driver versions. These airflow measurements were better than past benchmarks used by speakers of previous generations. Ideally, the airflow through the seal would be 0*ccm* (airtight)

but the reality is that mating surfaces are not perfectly smooth so air will always find its way through the micro gaps, even when rubber gaskets are used.

The next verification was gasket sealing performance under 1*m* of water. An assembly composed of two passives, two passive gaskets and one printed housing were submerged according to IPX7 requirements (1*m* submersion for 30 minutes, Fig. 28). The results showed that no water was found inside the housing. Litmus paper was placed adjacent to the gasket to detect if any water from the tank crossed the gasket sealing. The paper was still dry upon inspection (Fig. 29). All hardness successfully sealed out water.

Fig. 28. Housing assembly submerged in testing tank

Next was the task of determining the amount of height margin. With the housing fixture still attached to the flowmeter and pressure tank, the fixture was placed under the Zwick load cell. The steel wires were removed so now the compression force is provided by the Zwick load cell, as before. Now the load cell is moved upwards from the assembled state, uncompressing the gasket, until the flowmeter gives a reading of 5*ccm* air leak, with internal air pressure set at 0.5*psi*. The amount of upward movement is the initial height margin and it is recorded for each gasket hardness. 30A=0.75*mm*, 40A=0.8*mm*, 50A=0.85*mm*, and 60A=0.9*mm*. These values make sense since stiffer gaskets provides more compression force and so air cannot leak as fast until the stiff gasket is uncompressed further.

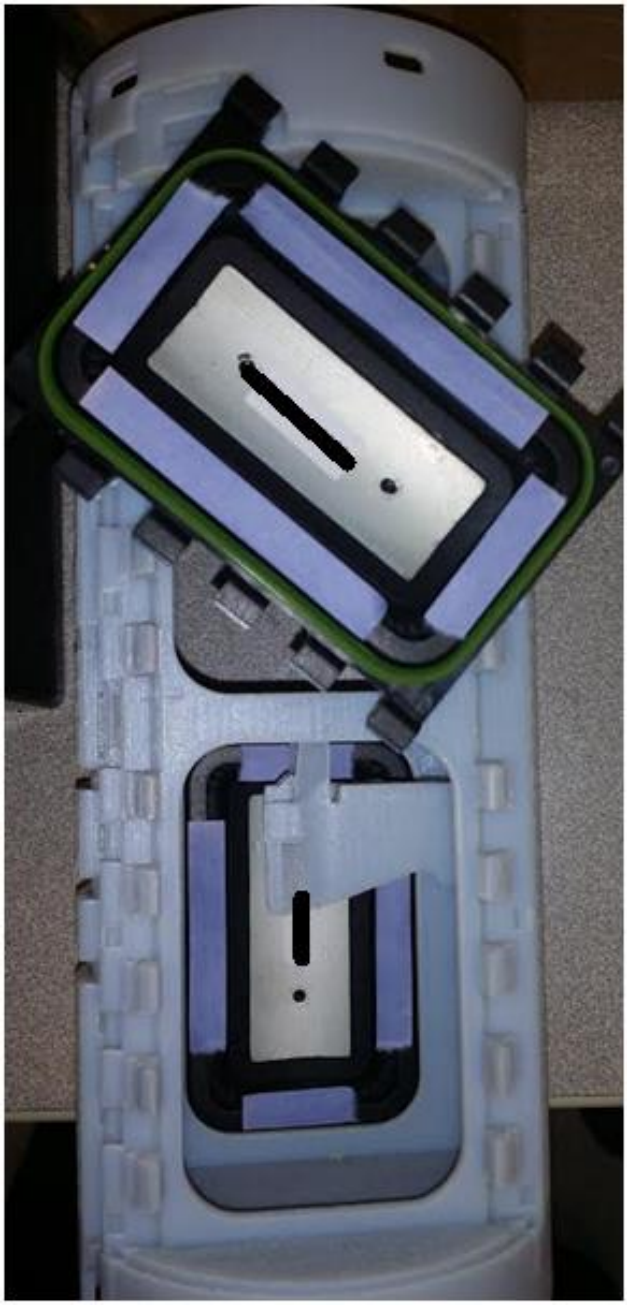

Fig. 29. Housing assembly remained dry inside

The sealing margin is arbitrarily defined as when the gasket is leaking air at a rate of 5*ccm*, measured using the Zwick and flowmeter. When comparing the height margin values against simulation, it appears that a force of $0.05N$ per *mm* length of gasket is necessary to prevent excessive air leak. This force value may then be used as the limit for determining sealing

margins in the simulation. This is a good illustration of how simulation and experimental testing can work together to solve for the unknown variables.

Next, a modified housing fixture was printed to repeat the IPX7 test. This time, the housing had its sealing surface offset, such that the compression was reduced by 0.75*mm*. Another way to say this is that the gland depth was increased by 0.75*mm*. The goal of this test was to check if the initial sealing height identified by a 5*ccm* air leak is a good conservative indicator of water sealing ability. All gasket hardnesses were tested and all passed at 0.75*mm*. Additional fixtures were printed with 0.8, 0.85, and 0.9*mm* increased gland depth. Further IPX7 testing confirmed the initial water sealing margins identified from air leak testing were valid. 30A=0.75*mm*, 40A=0.8*mm*, 50A=0.85*mm*, and 60A=0.9*mm*. This confirmed the correlation between air sealing performance and water sealing performance. Simulation data suggested the initial height margin was 1.1*mm* but the reality is that surfaces are not perfectly flat and free of particles, so the actual height margin is less than the ideal.

Later in the product development cycle, full speaker units were assembled during the pilot build phases. Twenty units were reserved to be heated to 70°*C* and immersed in water, in accordance with "thermal IPX7" testing procedure. It should be noted that manufacturing tolerances made it difficult to compare real world results with simulation results. The nominal housing sealing surface is completely flat but the reality is that high and low spots existed on the housing, as a result of molded part warpage. Such warpage is common and unavoidable. Despite this difficulty, a comparison of creep behavior was made. Before thermal exposure, the gap at the center of the center housing beam measured 1.9*mm* on average. After thermal exposure, the gap measured 2.25*mm* on average, for a creep strain increase of 0.35*mm*. Since, the expected creep - strain from simulation was 0.4*mm*, the actual creep strain fell within expectations. This

verification step also highlights why $0.2mm$ of manufacturing tolerance must be built into the design. Extensive thermal IPX7 testing was conducted prior to product launch, and those tests confirmed the seal design remained waterproof after creep effects.

CHAPTER SIX: SURFACE IMPERFECTIONS

Although the rubber gasket should ideally be able to close the flow paths between parts, surface defects can sometimes defeat the rubber gasket seal even with adequate sealing pressure. Surfaces that are too rough make it difficult for the rubber to fill in the valleys. Similarly, surfaces that have scratches also challenge the rubber to fill the void. Particulates that find their way between the rubber seal and the mating part will create air gaps. Similarly, steps on the mating surface will also create air gaps. Simulation may be used to examine the size of these air gaps. Fig. 30 below illustrates these 4 defect types.

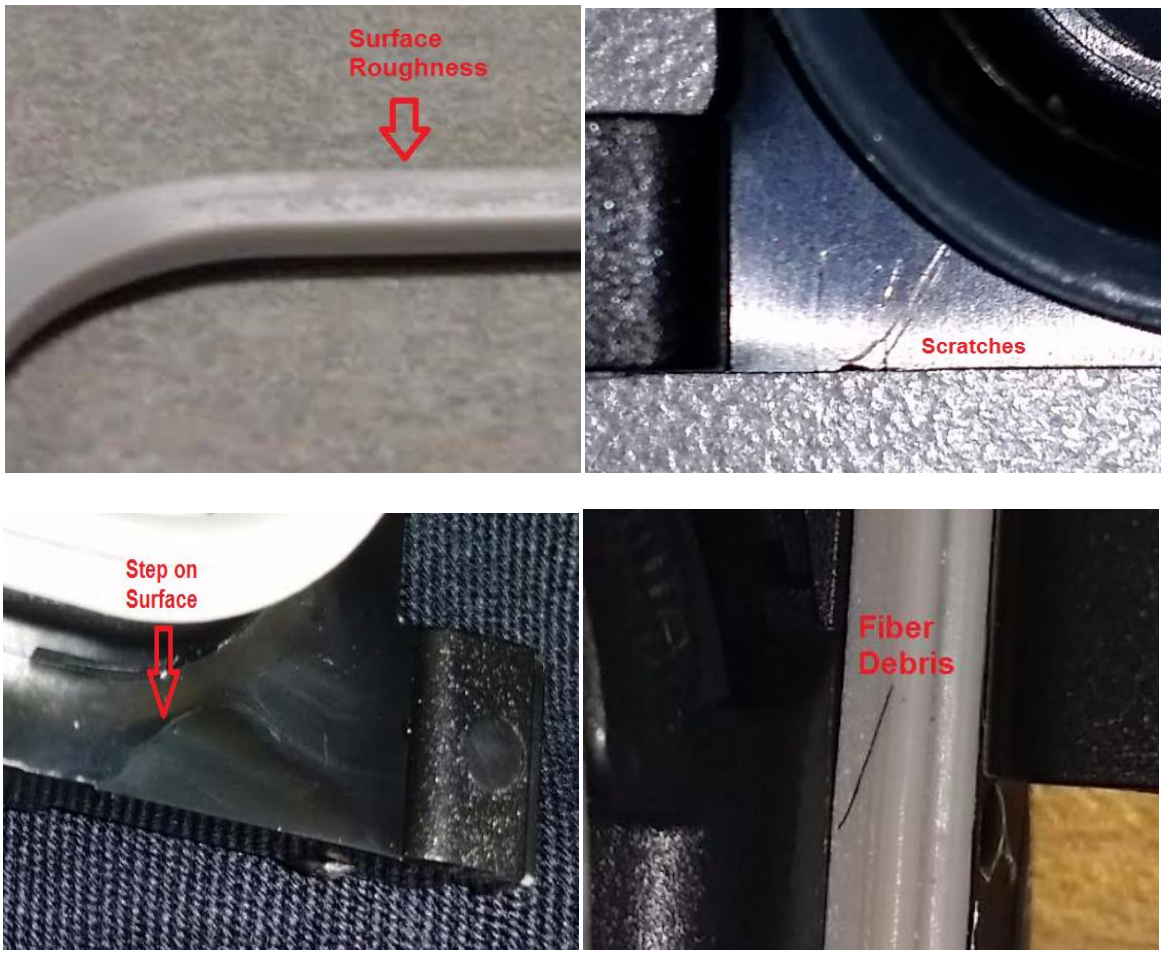

Fig. 30. Four types of defects that can defeat sealing.

These imperfections all allow leakage by the same mechanism, which is the formation of micro leak paths at the seal-substrate interface. Persson and Yang [27] studied the effects of roughness induced leakage, based on percolation theory. A leak path forms when the contact area is less than 40% of the total sealing area. The area % that sees contact is proportional to the contact pressure and inversely proportional to the roughness of the substrate. Therefore, it is more difficult to establish sufficient sealing contact area when working with rough surfaces. The length scale of rough surfaces is often smaller than $0.1mm$ and random, making it very expensive to simulate such fine features in Ansys. Persson and Yang's theory of sealing suggest that the flowrate is strongly dependent on the squeezing pressure, as shown in Fig. 31.

Since in our case study, the roughness of the ABS mating surfaces is specified as SPI-A2, the rms roughness should be smaller than $0.05\mu m$. Also, the sealing pressure does not fall below $0.05MPa$ in simulation. Therefore, the leak rate of our sealing system should always be less than 1E-13 m^3/s or 6E-6 *ccm* or 1.8E-4 *cc* over 30 *mins*. Such small leak rates would be acceptable for IPX7 requirements. Further work done by Lorenz and Persson [28] suggests that seals may be leak proof even when the contact area is below 40% when accounting for the elasticity of the rubber seal. Contact regions tend to merge together under the influence of contact pressure, isolating leak path regions.

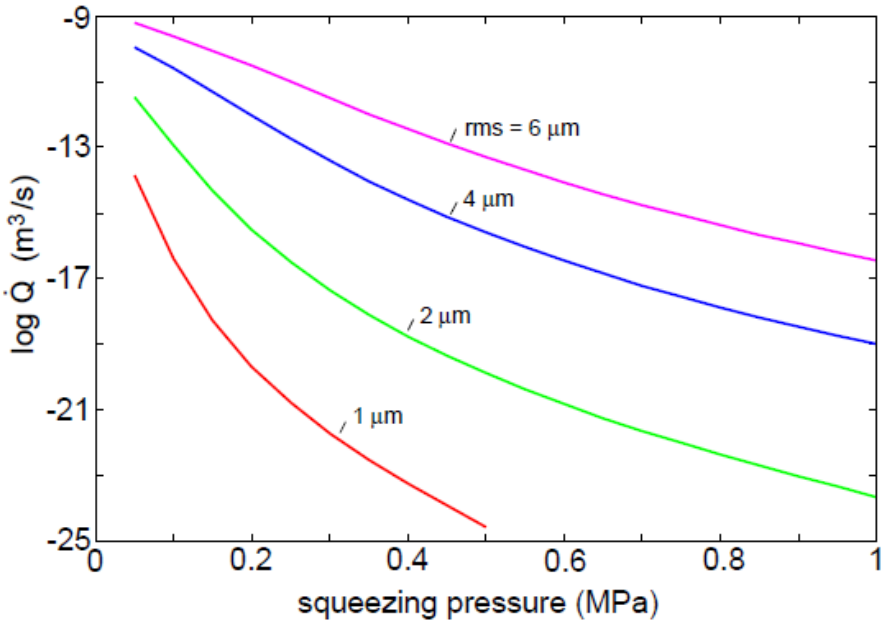

Fig. 31. The water ingress rate Q as a function of squeezing pressure P_0 and surface roughness. The fluid pressure is 0.01 MPa. [27]

It would seem that surface roughness is not really problematic for sealing but scratches from mishandling could easily be 0.5mm wide and 0.2mm deep, for example, and cause sealing failure. When detected, the parts with scratches must be scrapped and better handling procedures implemented. In the case of debris, it is difficult to remove airborne particles from the air completely without the use of a cleanroom, which would be too costly to implement. At what size would airborne debris be problematic for sealing? An experiment was conducted using human hair of various diameters placed across the sealing area. The point of leakage was observed and simulation was run to visualize the size of the leak path that allowed water ingress. The gasket that is studied in this experiment has a different shape than the previous gasket.

To carry out the failure analysis experiment, clear acrylic blocks were machined to allow visual inspection of the seal. The silicone gasket is placed onto the acrylic part in the same configuration as is done on the speaker product. Hairs of varying sizes are then placed perpendicular to the perimeter of the seal, as shown in Fig. 32. Where the gasket makes higher pressure contact with the acrylic part, there appears a shading on the gasket surface. In Fig. 33, notice how the hair interrupts the gasket's contact to the acrylic part.

Fig. 32. Hair is placed onto the sealing surface, perpendicular to the seal perimeter.

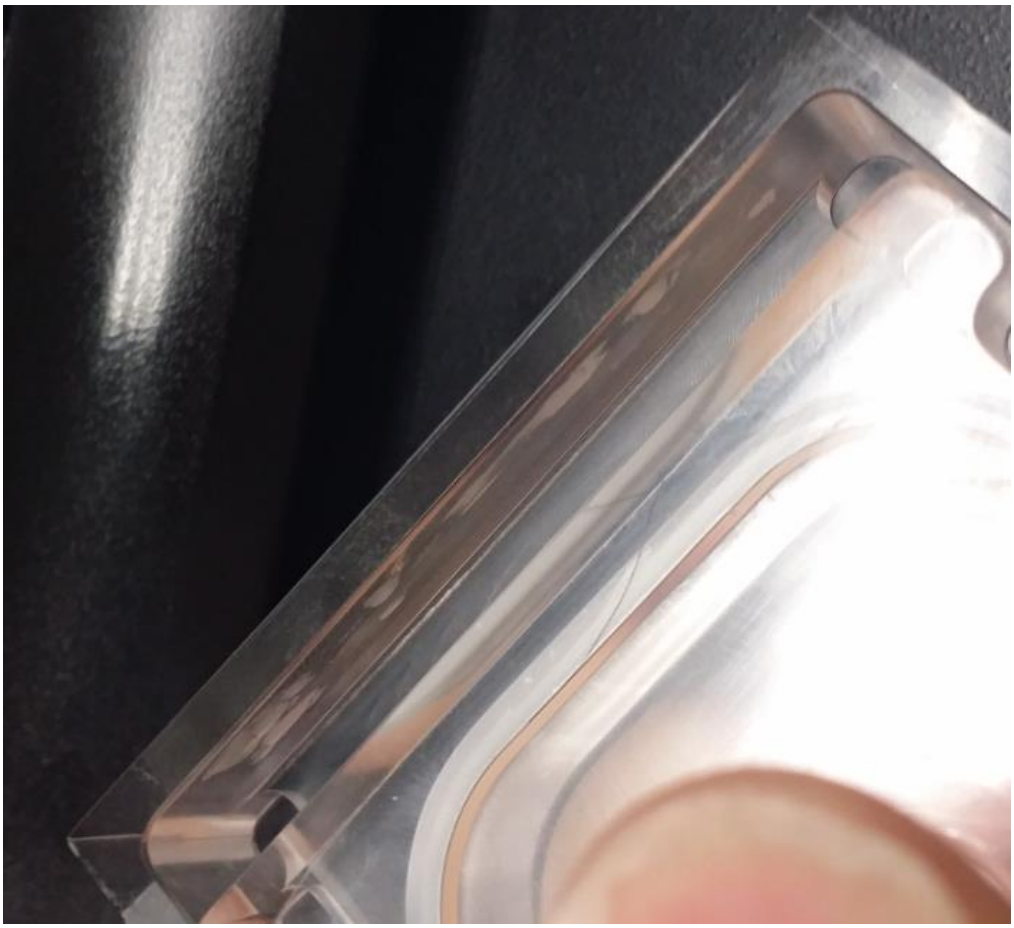

Fig. 33. Gasket sealing area (dark gray) is interrupted by hair.

The top acrylic part is captured in a drill chuck which is attached to a Zwick Roell uniaxial force-displacement measurement machine (Fig. 34). The bottom acrylic part has a hose attachment that allows application of vacuum pressure to the internal air chamber. This vacuum pressure acts to pull in water into the air chamber if a leak path exists. 10kPa of vacuum pressure is used to mimic the effect of submerging a speaker under water at a depth of 1m.

Before the water ingress testing is started, a bubble test is conducted to verify that the only available leak path is at the location of the hair (Fig. 35). This is done to ensure there are no other leak paths that may contribute to the water ingress. The bubble is produced by pressurizing the internal air chamber, forcing air into the water volume.

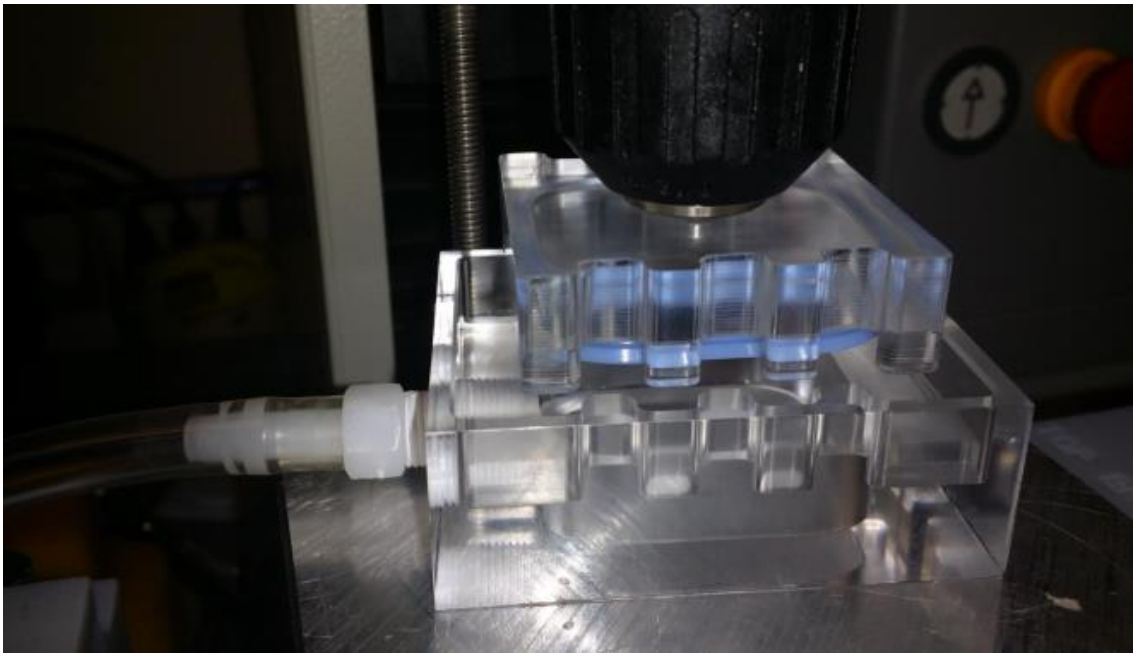

Fig. 34. Two acrylic blocks set up to compress a silicone gasket.

Fig. 35. Pressurized air produces a bubble at only the hair location.

After the bubble test is completed, the air hose gets switched to vacuum pressure and 60 seconds are allowed to pass, to see if the water breaches the seal. If no water has breached, then the top acrylic part is raised incrementally and another 60 seconds are allowed to pass. This is repeated until water ingress is observed. It is interesting that the water ingress tended to flow along the perimeter of the seal before it pooled into a droplet at the corner of the acrylic part (Fig. 36).

Fig. 36. Water ingress spotted at the corner of the gasket seal.

The hair sizes were measured using a micrometer and the test samples measured 20, 26, 29, 35, 40, 45, and 55 microns in diameter. The hair sample size, along with the compression gap at which they failed is plotted below in Fig. 37. Notice how larger hairs failed earlier while smaller hairs could tolerate larger gaps, a difference of more than 0.5*mm*.

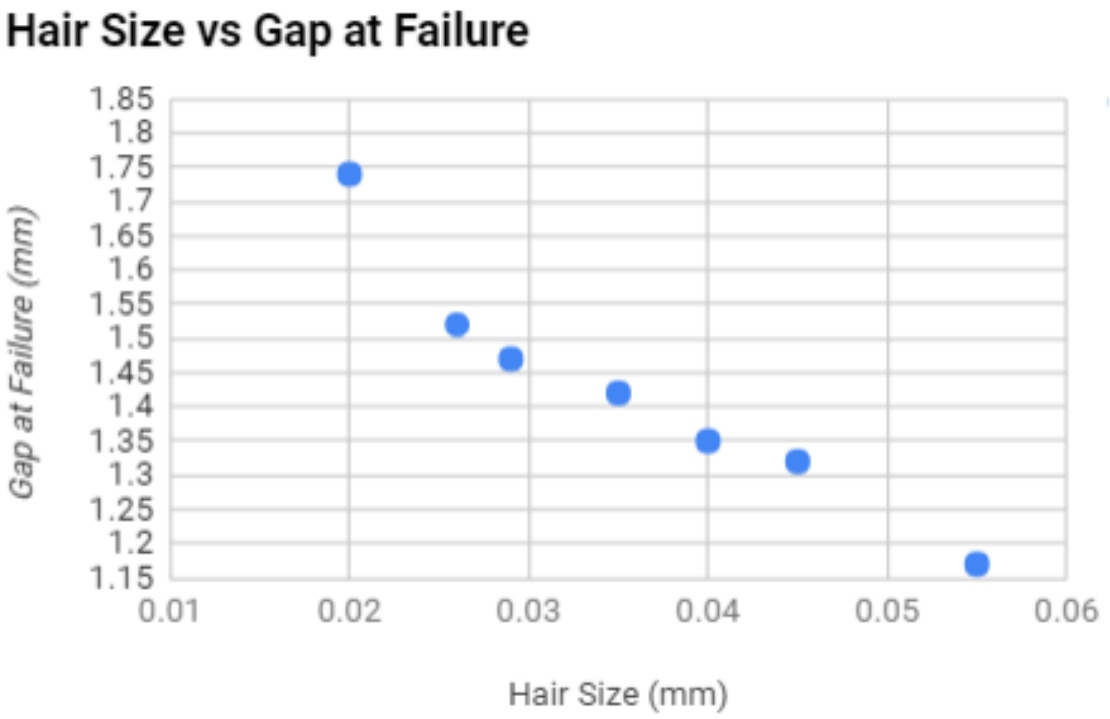

Fig. 37. Hair size vs gap at sealing failure.

The gap data was then used as input for simulation in order to see what size air gap allowed for the leak to occur. In the simulation model, Two ABS parts sandwich a silicone gasket, as shown in Fig. 38 below.

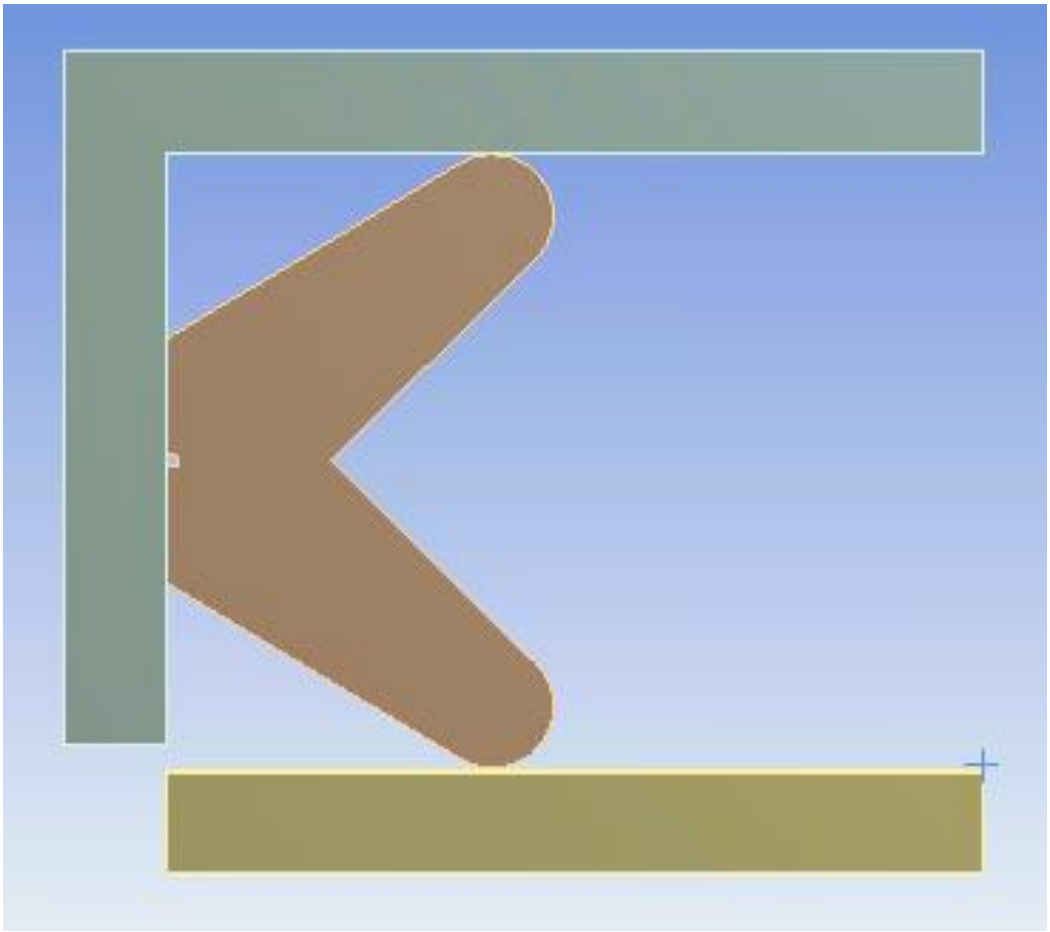

Fig. 38. Cross section view of two ABS plates compressing a silicone gasket.

Included in the bottom plastic part is a small bump in the sealing surface, used to model the presence of a hair (Fig. 39). The hair will be modeled at varying sizes, and its stiffness will be assumed to be close to that of ABS. Surface roughness defects are approximately 1 micron in size and therefore negligible when compared to the size of debris, which can range from 10 microns to 100 microns. Of course, there is no limit to the size of debris that may exist but larger debris is more easily spotted and removed, so their impact need not be studied. What is of interest is whether hairs below 100 microns can degrade sealing performance and by how much. Step defects and scratches also range in the 10 to 100 micron size so the hair defect is a good proxy for understanding step defects and scratches as well.

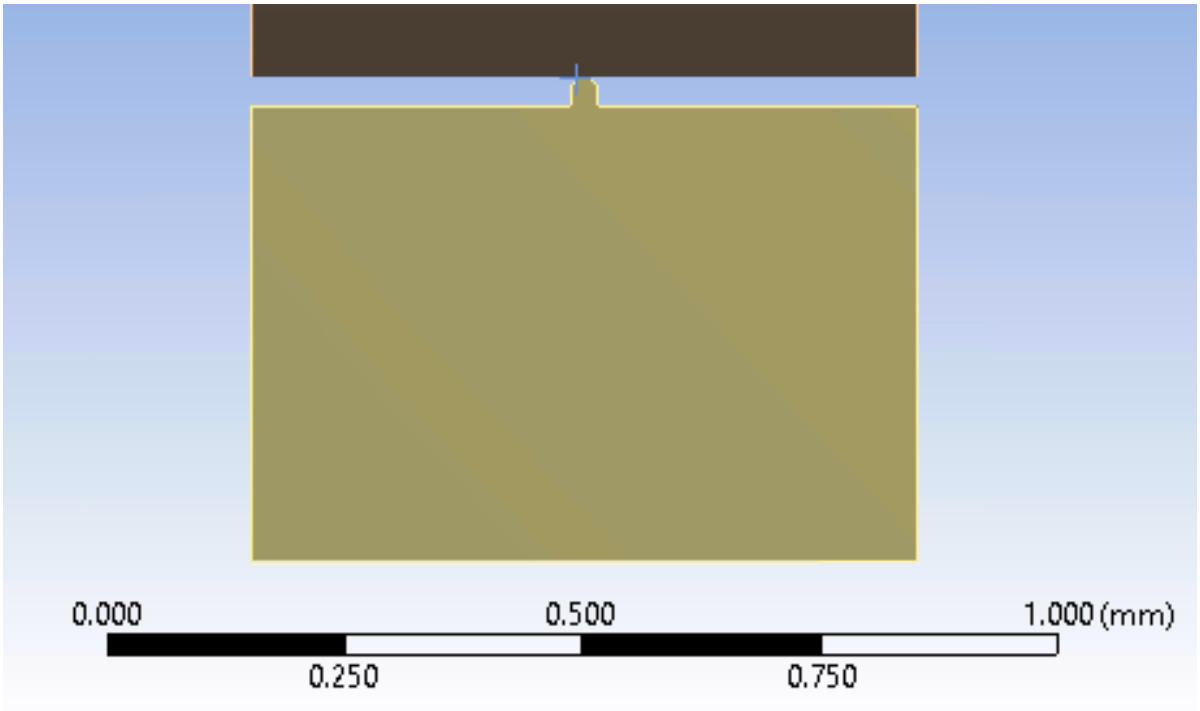

Fig. 39. Bump in bottom ABS part to represent hair debris.

The material properties and connections will be similar to the previous 2D simulation. Hex dominant method was used to model the ABS parts with a mesh size of 0.15*mm*. The gasket body was meshed with the sweep method using hex elements, sized at 0.1*mm*, with a face sizing refinement at the lower face. Those elements were sized at 0.03*mm*. The hair feature was given an edge sizing of 0.05*mm* (Fig. 40).

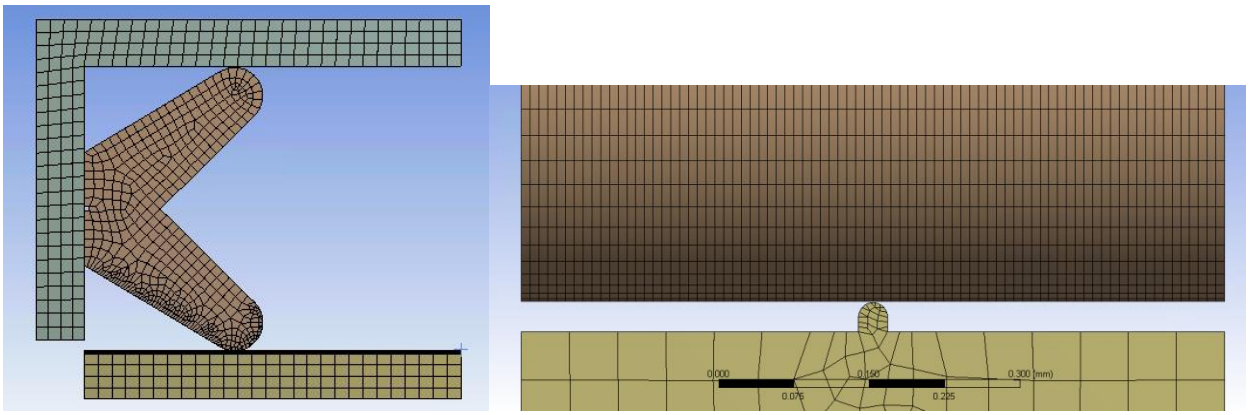

Fig. 40. Mesh setup used for simulation.

The upper ABS part is fixed while the lower ABS part is moved upward a distance of 1.9mm using a displacement condition. The silicone gasket has a frictionless support constraint on its left surface to represent the tension force of the gasket, holding the gasket onto its frame, which is presented by the left wall (Fig. 41).

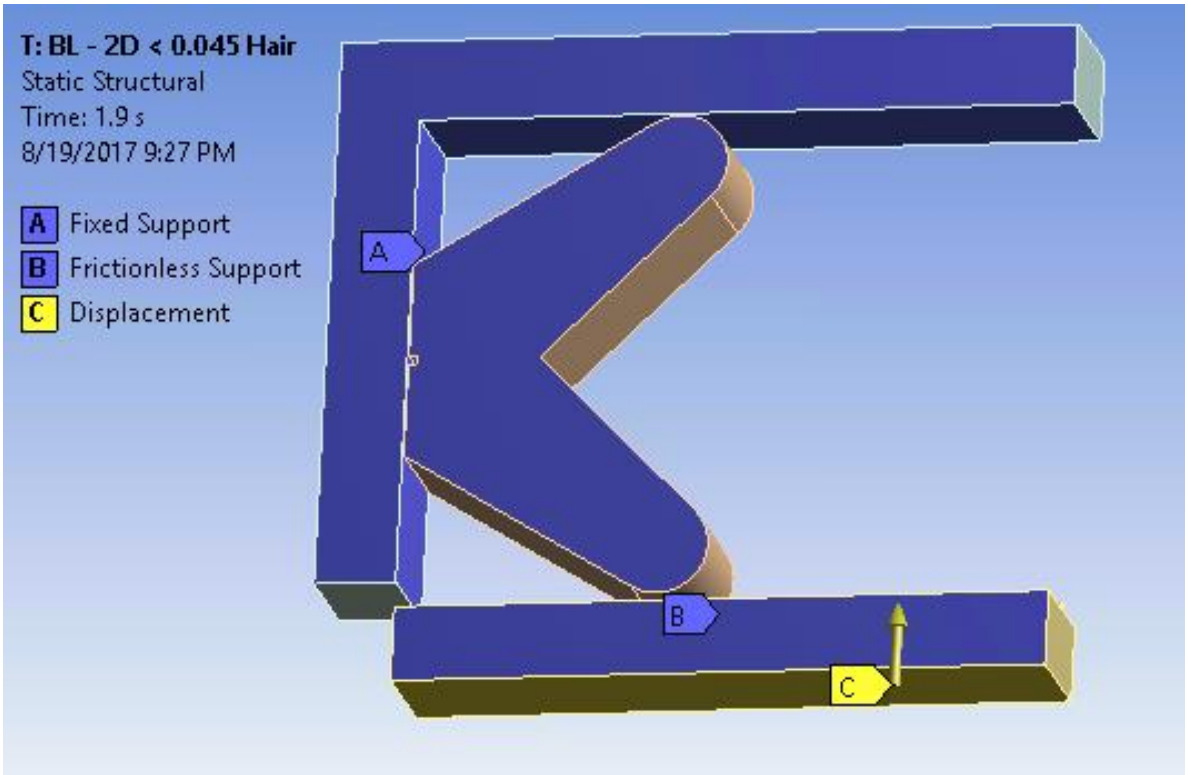

Fig. 41. Boundary conditions used in simulation.

Under the solutions branch, the resulting air gap and how it changes at various degrees of compression is of interest. Fig. 42 shows the gasket compressed over the 0.029*mm* hair at 1.2*mm* of compression and 1.7*mm* of compression.

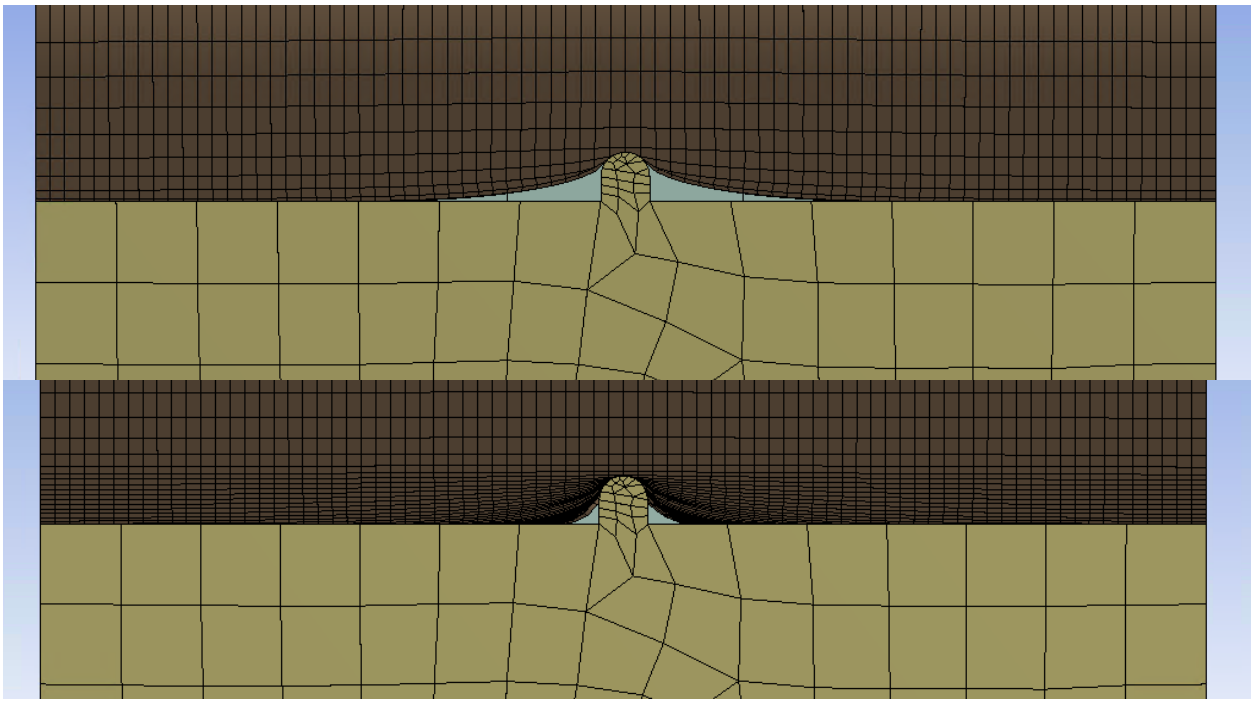

Fig. 42. Gasket compressed over 29 micron hair at

1.2*mm* (top) and 1.7*mm* (bottom) of compression.

The resulting geometries show air gaps that are triangular in shape, as can be expected. They also appear to be smaller as more compression is applied, as expected. In the designed compression state, the air gap diameter is around 12 microns. According to surface tension theory, the largest acceptable diameter that doesn't allow 10k*Pa* pressurized water to flow would be 29 microns, but this theory assumes that the geometry is flow out of a cylindrical capillary hole. What is the largest diameter air gap that is still acceptable in this scenario? Physical testing is required to determine when water flow occurs. From the experimental data gathered earlier, the gap-at-failure values can be input into simulation and the cross-section of the leak path can be measured (Fig. 43).

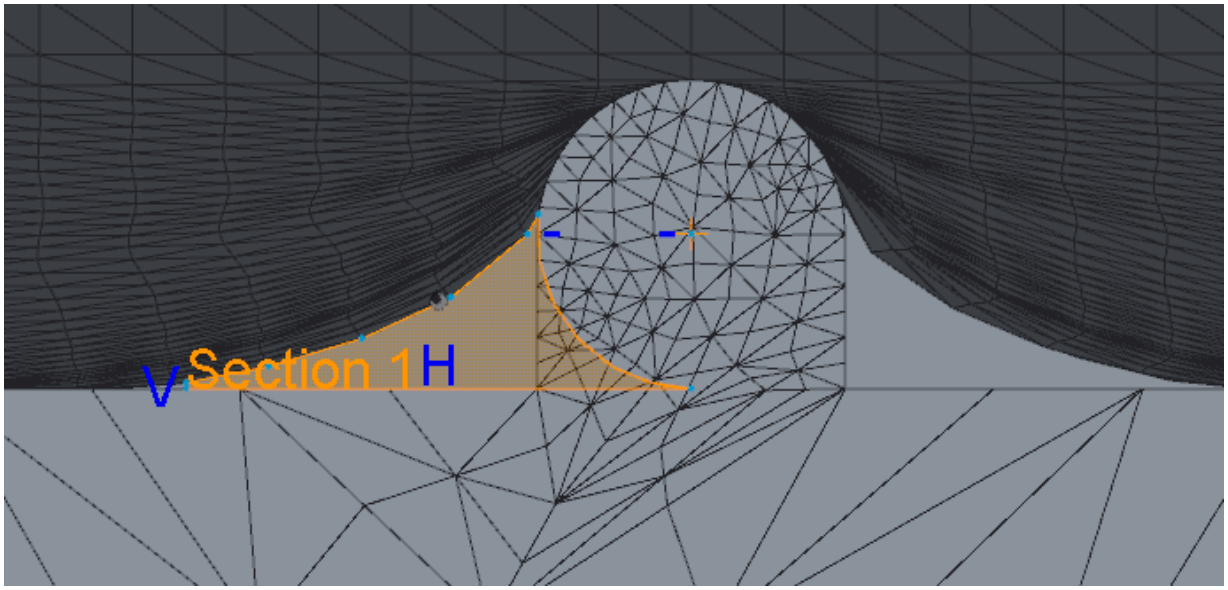

Fig. 43. The cross-sectional area of the air leak path that allows 10k*Pa* pressurized water to flow.

Areas and perimeters of the leak path were calculated to allow for the calculation of the hydraulic diameter. A table of results is shown below.

Table 3. Air gap size that allowed water flow for various trapped hair sizes.

Hair diameter (*mm*)	Gap (*mm*)	Area (*mm*^2)	Perimeter (*mm*)	Hydraulic Diameter (*mm*)
0.02	1.74	0.000393	0.157	0.0100
0.026	1.52	0.000232	0.103	0.0090
0.029	1.47	0.000235	0.098	0.0096
0.035	1.42	0.000279	0.110	0.0102
0.04	1.35	0.000290	0.113	0.0103
0.045	1.32	0.000323	0.119	0.0108
0.055	1.17	0.000307	0.116	0.0106

As can be seen from the table, hydraulic diameters larger than 9 microns allowed water ingress. This is lower than the theoretical size of 27 microns that is cited for flow out of a capillary hole. In this case, the geometry of the flow front just before ingress initiation is quite a bit more complex than the flow out of a circular tube. The screenshot below shows the geometry (Fig. 44.)

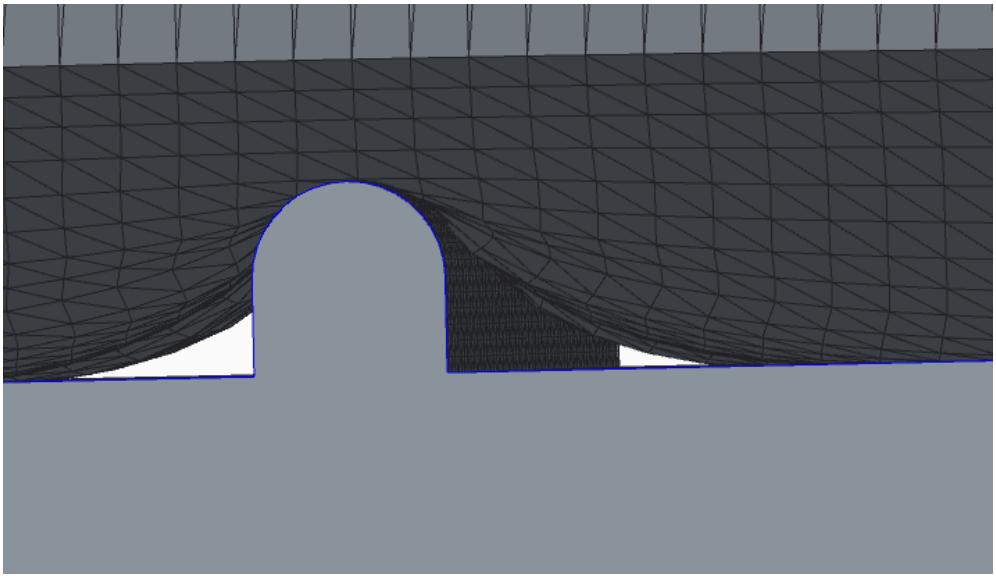

Fig. 44. View of the air leak path on both sides of the trapped hair.

Because the flow path gets wider towards the exit, surface tension opposes the flow since it acts to reduce the surface area of the flow front. It is concluded that at the initiation of water ingress, this surface tension must be exactly equal to the vacuum pressure of 10k*Pa*.

Given that the smallest hairs can degrade height margin so dramatically, it is critical to remove debris from the seal surfaces to a certain degree, which could be accomplished by means of pressurized air blowers. Because the speaker's sealing performance can be compromised by such small airborne particles that are hard to detect, how can the factory be certain of the sealing performance without actually submerging the product per the IPX7 test? Many have proposed an airleak check as a non-destructive substitute for checking water tightness. Based on earlier results seen, some small leak paths are not large enough to let water flow, due to water's surface tension, but would easily let air flow through. Hundreds of small leak paths would add up to a large airleak value and yet could all be watertight. And yet one large leak path may not allow much air to leak but would allow water to flow into the product. Because of this reality, it would seem impossible to specify a corresponding airleak criteria that would identify IPX7 suitability.

The methods of airleak measurement and techniques for setting some pass-fail criteria are described below.

Pregelj et al. [29] provides a summary of the various leak detection methods. The simplest of these methods is the bubble test which involves pressurization of the speaker with atmospheric air and submersion of the speaker under water. Air bubbles would then appear in locations where leak paths are present. In our case study, because there are several layers of cosmetic coverings, bubbles appearing at the exterior of the product do not give precise data about the leak location origins nor the size of each leak. The only data that can be known is the air leak rate passing through the speaker.

Cincinnati test systems [30] describe a method for establishing an air leak rate limit for meeting IPX7 requirements. They suggest collecting a number of parts that have various air leak rates and to test those parts for waterproofness. The part with the highest air leak rate that doesn't leak water should be used as the pass-fail limit. As more waterproof test data becomes available, the air leak rate limit can be tightened if too many IPX7 failures are seen in the field. This method represents a statistical approach to setting an air leak limit but in reality, no air leak limit can 100% screen out speaker assemblies that would fail IPX7, except very tight leak limits. The problem with very tight limits is that it would screen out too many speaker assemblies that are actually watertight. In practice, the airleak screening can be used to detect and screen out gross leaks, but does not guarantee that 100% of units with a low air leak will be watertight. This is because the airleak rate and water tightness are not 100% correlated.

CHAPTER SEVEN: CONCLUSION

The product design problem of waterproofing a portable speaker was examined in this research and the solution process detailed. With the aid of simulation, a gasket seal design was developed in this study. By understanding that the primary failure mode was loss of compression by thermal creep, steps were taken to reduce creep by reducing compression forces. At the same time, the concept of height margin was developed to compare different gasket designs against one another. Not only should the ideal gasket design produce minimal creep, it should also be able to seal against the maximum creep. That is, it should have so much initial height margin, that despite a high creep strain, the final height margin would still be adequate. A 2D gasket cross section was studied to reduce optimization time, and the best performing shape was transferred to the full 3D model. There, assembly forces were measured, as well as contact pressures and creep strain. Additional improvements were made to the frames and housing to build up height margin. Experimental testing validated the deformation behavior of the gasket, the force reaction, the stick-slip sliding behavior, the contact pressure band, and the fact that the gasket sealed with at least $0.75mm$ of initial height margin. Creep testing confirmed that the amount of strain matched simulation and extensive IPX7 testing after creep effects gave 100% passing results during the final pilot build. As more consumer electronics are becoming waterproof, the methods for achieving efficient waterproof designs are becoming more in demand. Simulation of this rubber gasket allowed the study of the sealing mechanism to gain insight, trial ideas, and ultimately achieve a waterproof design that is also heat resistant.

The influence of surface imperfections on sealing performance was also analyzed. Using simulation, it is possible to visualize the resulting air gaps caused by hairs trapped between the gasket seal and plastic surface. Through experimental testing, the gaps at which the seals failed

at were discovered, which was dependent on the size of the trapped hair. This gap failure data was used in simulation to measure the smallest cross section of the leak flow path and compute the hydraulic diameter. Hydraulic diameters larger than 9 microns were found to allow water ingress. This value differed from the theoretical value for flow out of a capillary hole, because the geometry of the flow path is different. Because such small hairs can affect sealing performance and because their presence is difficult to detect, air cleaning stations are needed to remove the majority of debris as a preventative measure. Secondly, a final air leak check of the speaker product may be used to screen grossly leaking product. Although the screening cannot be 100% effective in theory, it has proven effective enough for practical purposes, as very few returns are seen related to water-damage.

REFERENCES

[1] H. K. Muller, B. S. Nau, Fluid Sealing Technology: Principles and Applications, Marcel Dekker, Inc., New York, 1998.

[2] Blue Sea Systems, IP (Ingress Protection) Ratings. Webpage. (2014).

[3] C.C Leea, K.N. Chianga, W.K. Chenb, R.S. Chenb, Design and analysis of gasket sealing of cylinder head under engine operation conditions, Finite Elements in Analysis and Design, 41(2005)1160-1174 .

[4] X. Bao, P. Younse, Finite element analysis of seal mechanism using SMA for Mars sample return, Proc. SPIE 9061, Sensors and Smart Structures Technologies for Civil, Mechanical, and Aerospace Systems (2014).

[5] F. Yun, et al., Analytical and experimental study on sealing contact characteristics of subsea collet connectors, Advances in Mechanical Engineering. 9-4(2017)1-14.

[6] M. Bharadwaj, et al., Modeling Creep Relaxation of Polytetrafluorethylene Gaskets for Finite Element Analysis, International Journal of Materials, Mechanics and Manufacturing. 5-2(2017)123-126 .

[7] K. Maekawa, T. Obikawa, Y. Yamane, Mechanical Design, Elsevier Science, 2003.

[8] H. P. Bloch, Pump Wisdom : Problem Solving for Operators and Specialists. Wiley, 2011.

[9] S. Rapra, High Performance Elastomers and Polymers for Oil and Gas Applications 2012., Smithers Rapra, Britain, 2012.

[10] R.J.F Goodfellow, Concrete for Underground Structures : Guidelines for Design and Construction, SME, 2011.

[11] K.M. Gupta, Material Science and Engineering Technology II, Trans Tech Publishers, Zurich, 2013.

[12] T.J. Hovland, M. Najafi, Inspecting Pipeline Installation. ASCE, Virginia, 2009.

[13] S. Engelmann, Wiley Series on Polymer Engineering and Technology : Advanced Thermoforming : Methods, Machines and Materials, Applications and Automation. Wiley, New Jersey, 2012.

[14] L. Bachus, A. Custodio, Know and Understand Centrifugal Pumps. Elsevier Science, 2003.

[15] S. Rapra, Oilfield Engineering with Polymers, Smithers Rapra, Britain, 2006.

[16] R.P. Brown, Rubber Product Failure. Smithers Rapra, Britain, 2002.

[17] R. Smith, R.K. Mobley, Industrial Machinery Repair, Elsevier Science, 2003.

[18] M.D. Holloway et al., Process Plant Equipment : Operation, Control, and Reliability. Wiley, 2012.

[19] W. Swete, Rod seal is designed to meet the toughest demands of hydraulic equipment, Sealing Technology, 8(2016)9-10.

[20] SKF, Seals designed to meet the challenges of the wind-energy industry, Sealing Technology, 2(2016)8.

[21] A. Zahorulko, Experimental investigation of mechanical properties of stuffing box packings, Sealing Technology, 8(2015)7-13

[22] H. K. Muller, B. S. Nau, Fluid Sealing Technology: Principles and Applications, Marcel Dekker, Inc., New York, 1998.

[23] Shin-Etsu, Characteristic properties of Silicone Rubber Compounds. Webpage. (2008).

[24] Apple Rubber, Seal Design Guide. Webpage. (2009)

[25] C. Carmody, Explosive decompression and other O-ring-related issues for turbomachinery service – guidance for users, Sealing Technology, 12(2015)8-12.

[26] ANSYS, User Guide, Lecture 4: Hyperelasticity, (16 April 2015).

[27] B. N. J Persson, C. Yang, Theory of the leak-rate of seals, Journal of Physics: Condensed Matter, 20-31(2008).

[28] B. Lorenz, B. N. J Persson, Leak Rate of Seals: Effective-Medium Theory and Comparison with Experiment, Eur. Phys. J. E, 31-159(2010).

[29] A. Pregelj, M. Drab, M. Mozetic, Leak Detection Methods and Defining the Sizes of Leaks, The 4th International Conference of Slovenian Society for Nondestructive Testing "Application of Contemporary Nondestructive Testing in Engineering", (1997).

[30] Cincinnati Test Systems, How to Establish Acceptable Leak Rate Criteria for Automated Testing, Application Bulletin #120 (2009).